

New resveratrol derivatives as improved biologically active structures: design, synthesis and computational modeling

Milena Mlakić ¹, Ilijana Odak ^{2,*}, Danijela Barić ³, Stanislava Talić ², Ivana Šagud ⁴, Zoran Štefanić ⁵, Krešimir Molčanov ⁵, Zlata Lasić ⁶, Borislav Kovačević ^{3,*} and Irena Škorić ¹

¹Department of Organic Chemistry, Faculty of Chemical Engineering and Technology, University of Zagreb, Marulićev trg 19, HR-10 000 Zagreb, Croatia

²Department of Chemistry, Faculty of Science and Education, University of Mostar, Matice hrvatske bb, 88 000 Mostar, Bosnia and Herzegovina

³Group for Computational Life Sciences, Division of Physical Chemistry, Ruđer Bošković Institute, Bijenička cesta 54, HR-10 000 Zagreb, Croatia

⁴Croatian Agency for Medicinal Products and Medical Devices, Ksaverska Cesta 4, HR-10 000 Zagreb, Croatia; Ivana.Sagud@halmed.hr

⁵Division of Physical Chemistry, Rudjer Bošković Institute, Bijenička cesta 54, HR-10 000 Zagreb, Croatia

⁶Teva api Analytical R&D, Pliva, Prilaz Baruna Filipovića 25, HR-10 000 Zagreb, Croatia

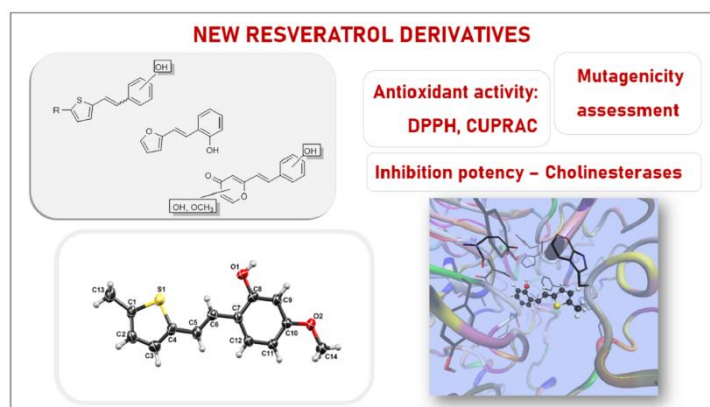
*Correspondence: Prof Ilijana Odak; ilijana.odak@fpmoz.sum.ba; Dr Borislav Kovačević; Borislav.Kovacevic@irb.hr

Abstract: New derivatives of the well-known bioactive trihydroxy-stilbene resveratrol were synthesized to investigate their potential biological activity. The focus was on assessing their ability to inhibit cholinesterase enzymes (ChEs) and their antioxidative properties, which were thoroughly examined. New resveratrol analogs were synthesized through Wittig or McMurry reaction in moderate-to-good yields. In all synthetic pathways, mixtures of *cis*- and *trans*-isomers were obtained, then separated by chromatography, and *trans*-isomers were isolated as targeted structures. The stilbene derivatives underwent evaluation for antioxidant activity (AOA) using DPPH and CUPRAC assay, and their potential to inhibit acetylcholinesterase (AChE) and butyrylcholinesterase (BChE) was also measured. The biological tests have shown that the same compounds exhibited significant antioxidative and cholinesterase inhibitory potential, as evidenced by lower IC₅₀ values compared to the established standards, *trans*-resveratrol and galantamine,

respectively. Additionally, molecular docking of the selected synthesized potential inhibitors to the enzyme's active site was performed, followed by the assessment of the complex stability using molecular dynamics simulation lasting 100 nanoseconds. Lastly, the new compounds underwent examination to determine their potential mutagenicity.

Keywords: antioxidative activity, cholinesterase inhibition, computational modeling, resveratrol derivatives, synthesis

Graphical abstract



1. Introduction

To find new molecules that would retain structural stability and excellent therapeutic properties, great attention is paid to stilbenes and their derivatives, known for their excellent therapeutic effects [1]. **Most stilbene structures found in nature** have excellent therapeutic properties thanks to their antioxidant activity [2-4]. Stilbenes are found in various natural compounds, but most often in plants that synthesize them to protect themselves from adverse environmental **conditions**. **The** primary role of stilbene in plants is to protect cells from oxidative stress, and some of them also act as toxins against various pathogens [5].

Particularly interesting in this sense are their hydroxyl derivatives with an emphasis on the compound resveratrol (Figure 1) [6]. *Trans*-resveratrol (Figure 1) is a molecule that belongs to stilbenes and is the most famous hydroxy-derivative from this group of compounds. It is known to

act as an **antioxidant**, and according to the latest research, *trans*-resveratrol actively participates in several mechanisms in the pathology of Alzheimer's disease (AD) [7,8]. In the human body, *trans*-resveratrol is biosynthesized by the enzyme stilbene synthase [9,10], and it was found that it destroys and inhibits the formation of preformed aggregates, reduces the activation of microglia and the Sirtuin1 (Sirt1) biological pathway, which modulates the transmission of nerve signals in the body [11]. Despite the proven positive effects, further research is needed to prove the safety and functionality of *trans*-resveratrol in the human body. Due to the presence of the ethylene fragment within its structure, hydroxy-stilbenes exist as isomeric structures; that is, *cis*- and *trans*-configurations of each molecule are possible. When investigating isomeric forms of hydroxy-stilbenes and their biological potential, it should be kept in mind that *trans*-isomers are more often present in natural compounds and are more stable and biologically active than *cis*-isomers [5]. Most of the currently known biological active hydroxylated stilbene structures belong to *trans*-resveratrol derivatives (Figure 1).

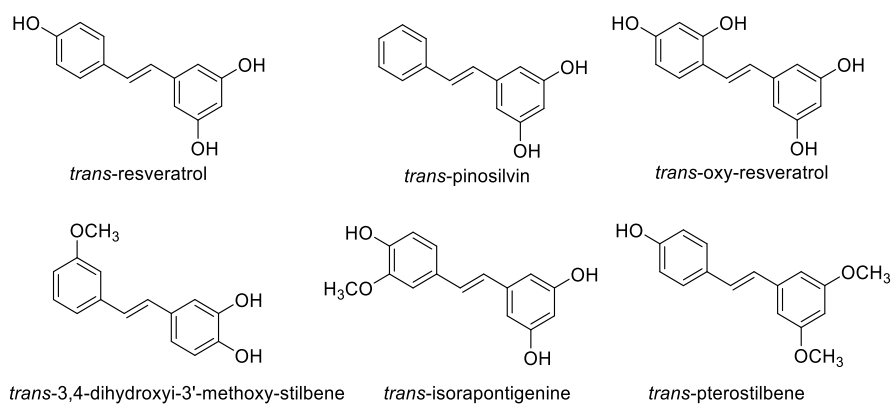


Figure 1. Representatives of hydroxy-stilbene derivatives with proven biological activity.

Numerous studies have shown that stilbene, and especially resveratrol and its **derivatives**, have a similar effect on human health and show pronounced antioxidant, antitumor, antimicrobial, anti-inflammatory, anti-neurodegenerative, antiviral, and antidiabetic properties [12]. In addition to the properties mentioned above, it has been shown that stilbenes and analogs act as luminophores due to the possibility of interaction with **radiation** [13,14].

Antioxidants are generally considered substances whose properties make it possible to slow down or even prevent the oxidation of biological substrates caused by reactive substances such as free radicals [15]. **As** a result of increasingly stressful living conditions in the human body, more and

more free radicals are formed, which then damage proteins, DNA, and lipids, leading to various diseases [16]. Mechanistically, the antioxidant activity is based on the antioxidant's ability to trap free radicals in the molecular skeleton and release hydrogen atoms. If a favorable functional groups and positions in the structure are chosen, the antioxidant activity can be increased with the appearance of new effects, such as improved diffusion through the cell membrane and bioavailability. *Trans*-resveratrol is proven as an agent that reduces changes in mitochondrial potential, thus inhibiting the accumulation of free radicals [17]. Because of this fact, hydroxy-stilbenes are recognized as a building block of great potential due to various possible structural modifications and the application of their therapeutic properties in medicine [5,18].

Hydroxy-stilbenes are also potentially used in treating Alzheimer's and Parkinson's diseases thanks to the possibility of synthesizing their small amphiphilic derivatives. The permeability of the blood-brain barrier (BBB) for amphiphilic derivatives exceeds the results for biological molecules investigated so far, precisely because of the differences in the hydrophobic and hydrophilic parts of the molecules, which further increase the binding affinity of hydroxy-stilbene to A β (β -amyloid) oligomers, which are one of the causes of continuous synaptic damage [19]. It has been proven that the natural polyphenol *trans*-resveratrol benefits the nervous system [20-22]. Resveratrol and its derivative pterostilbene (Figure 1) protect against dementia syndromes such as AD, as research on mammalian cells determined. Resveratrol has shown great potential in neurological protection, *in vitro* and *in vivo* research. It has been found to facilitate the breakdown of amyloid precursor protein and aid in removing neurotoxic amyloid- β peptides. It reduces damage to nerve cells by activating NAD⁺-dependent histone deacetylases known as sirtuins [23]. By increasing the resolution of β -amyloid and modulating intracellular effectors related to oxidative stress, neuronal energy homeostasis, apoptosis, and cell longevity, *trans*-resveratrol has an anti-neurodegenerative effect [24]. Testing on mice proved that *trans*-resveratrol protects neurons from polyglutamine (polyQ) toxicity in Huntington's disease and also from Wallerian degenerative decline in research [7]. Also, it acts as a neuroprotector in PC12 cells, protects against A β 25-35 induced toxicity, and weakens cell apoptosis [17].

Furthermore, *trans*-resveratrol is safe and well tolerated in patients with mild to moderate AD [25,26]. Since AD is characterized by low levels of acetylcholine in the patient's brain, current pharmacology is based on drugs that inhibit cholinesterases to enhance cholinergic neurotransmission. Oxidative stress is also an important aspect that must be considered in

neurodegenerative disease research. It can be concluded that hydroxy-stilbenes (especially *trans*-resveratrol) are very interesting in terms of multiple uses in therapeutic applications thanks to their biological action.

In our laboratory, in previous scientific research, thiophene analogs of hydroxy-stilbene, derivatives **1** and **2** (Figure 2), showed good biological activity [27], with potential inhibition of cholinesterase enzymes and high values for antioxidant activity. For the reason above, compounds **1** and **2** were used as a starting point for developing new resveratrol derivatives in this research. New compounds will be analyzed for their inhibitory effects on cholinesterase and antioxidant properties, making them an interesting new group of structures for further profiling as active components.

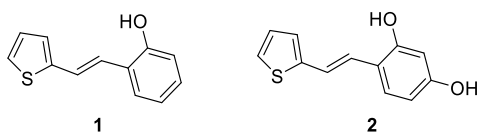


Figure 2. Structure of the previously investigated thiophene analogs of resveratrol (**1** and **2**) with proven antioxidant and cholinesterase inhibitory activity.

2. Results and Discussion

2.1. Synthesis and characterization of heteroaromatic resveratrol analogs **1-22**

In this research, heteroaromatic resveratrol derivatives **1-22** (Figure 3) with different number, position, and type of substituents on the aromatic and heteroaromatic rings were synthesized through several approaches (Scheme 1), with an emphasis on hydroxyl groups that significantly contribute to expected antioxidant activity and cholinesterase inhibition, and in combination with other substituents. Resveratrol derivatives **1** and **2** showed excellent antioxidant (DPPH) and inhibitory activity in previous research [27,28], but here, their antioxidation was also determined by another method for confirmation. The thiazole derivative **22** showed excellent inhibitory activity toward enzyme BChE [29], but exploring its antioxidation potential has not been conducted; therefore, in this research, we tested its inhibition towards AChE and its antioxidant potential using two methods, given that this is the only thiazole derivative.

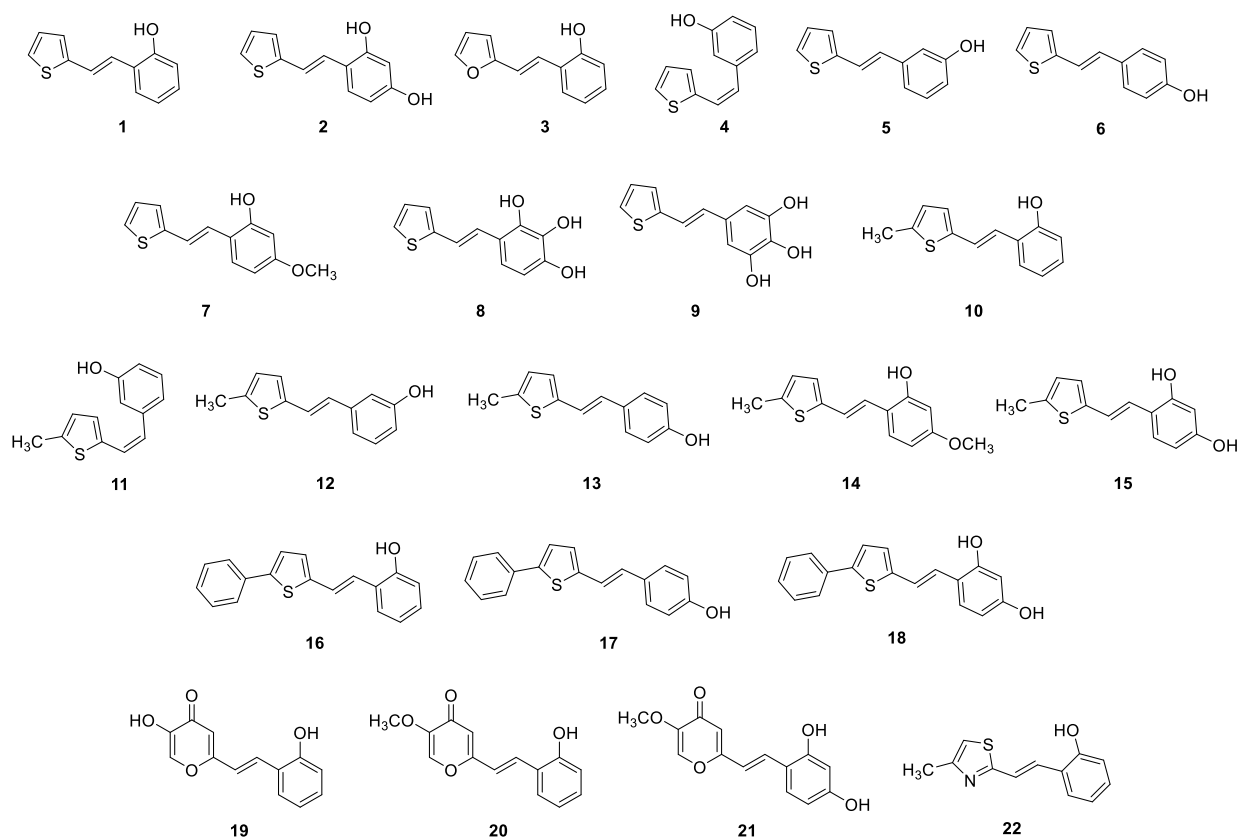
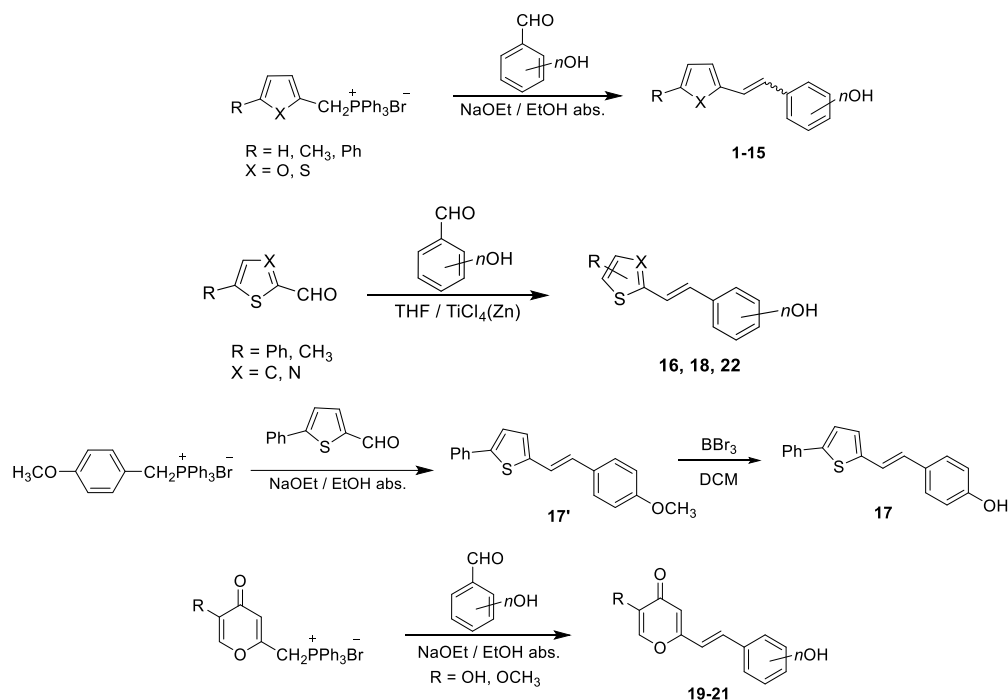


Figure 3. Structures of the synthesized hydroxyl-stilbenes **1-22**.

Resveratrol derivatives **1-15** were prepared by the Wittig reaction from phosphonium bromides and the different phenolic aldehydes. The Wittig reaction provided the new hydroxy-heterostilbenes **1-15**, preferably as mixtures of *cis*- and *trans*-isomers (mostly with very low proportions of *cis*-isomers in the mixtures up to 10%; see Experimental section). Mixtures of the geometrical isomers were separated to obtain pure *trans*-isomers by repeated column chromatography (in a wide range of isolated yields from 3% for resveratrol derivative **6** to 82% for compound **1**). Compounds **16**, **18**, and **22** were synthesized by the McMurry reaction (in 5%, 10%, and 12% of isolated yields, respectively) from the chosen aldehydes using zinc powder in THF and TiCl_4 . The organic product was purified on a column filled with silica gel. PE/E and PE/DCM solvent systems of different polarities were used as eluents. Compound **17** was synthesized starting from 4-methoxytoluene, NBS, and AIBN to give the corresponding *p*-methoxy-phosphonium salt used in the Wittig reaction with the proper aldehyde. By subsequent column chromatography, the pure **17'** was isolated in the last fractions used in the reaction with BBr_3 in DCM to produce pure

17 after column chromatography. Pyranone derivatives **19-21** were synthesized from the corresponding pyranone phosphonium salts and phenolic aldehydes in the Wittig reaction in low isolated yields due to the similar R_f values with the triphenylphosphine oxide as the second product. The **19-22** were isolated from the obtained raw products by successive column chromatography on silica gel, using PE/E and EtOAc/MeOH solvent systems of different polarities.



Scheme 1. Reaction pathways for the synthesis of new heteroaromatic resveratrol derivatives **1-22**.

Regarding synthesis and yield, it can generally be said that derivatives with OH groups in the *ortho*-position give higher isolated yields regardless of any other substituents (**1-3**, **7**, and **10**). With the substitution of the OH group in the *meta*-position, isolated yields are also satisfactory, but in this case, unlike *ortho*-substitution, *cis*-isomers predominate (**4**, **5**, **11**, and **12**). The *trans*-isomer predominates with the *para*-substituted OH group, but the yields are much lower than the previous one (**6** and **13**).

According to ¹H NMR spectroscopy, the position of the hydroxy group directs the yields and ratio of geometric isomers in the Wittig reaction. Among all the resveratrol analogs **1-22**, the ratio of *cis*- and *trans*-isomers, in most cases, the *trans*-isomer predominates in the reaction mixture, except when the hydroxyl group is in the *meta*-position on the benzene ring. Only then were the isolated yields on *cis*-isomers higher than for *trans*-isomers, and it was possible to isolate them (compounds

4 and **11**). In all the other cases, regardless of the reaction path, they were mainly obtained as *trans*-isomers (which are targeted), and *cis*-isomers could not be isolated as pure due to their small share in the reaction mixture.

All isolated heteroaromatic resveratrol analogs **1-22** are fully spectroscopically characterized (See ESI). In the ^1H NMR spectra of isolated resveratrol analogs **1-22**, it can be seen that the resolved patterns for ethylenic protons between 6.68 and 6.40 ppm (*cis*-isomers) and between 7.75 and 5.32 ppm (*trans*-isomers) with the characteristic coupling constants, the signals for the protons on various substituents and the signals for protons on the heteroaromatic and aryl rings (See for example Figure 4).

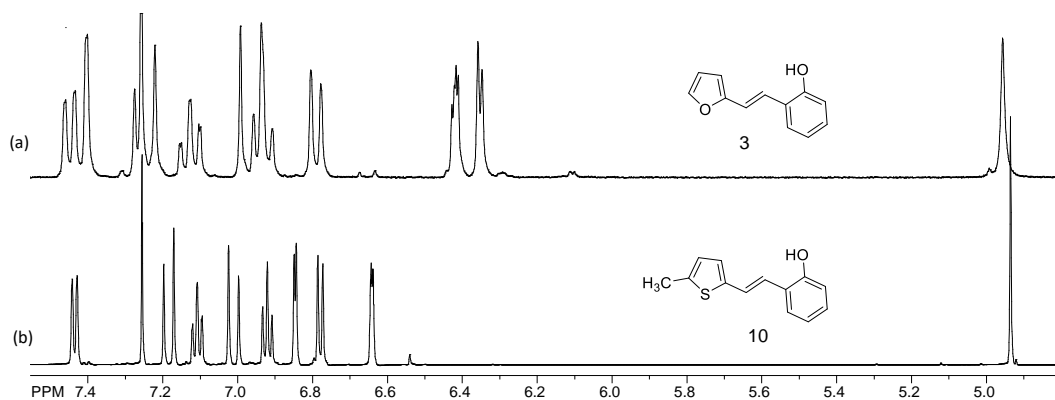


Figure 4. Parts of the ^1H NMR spectra of resveratrol analogs **3** (a) and **10** (b).

UV-Vis spectra in acetonitrile (Figure 5) of representatives of resveratrol derivatives are typical for diarylethene [30,31] with strong absorption with a maximum between 280 and 350 nm for all these presented *trans*-isomers.

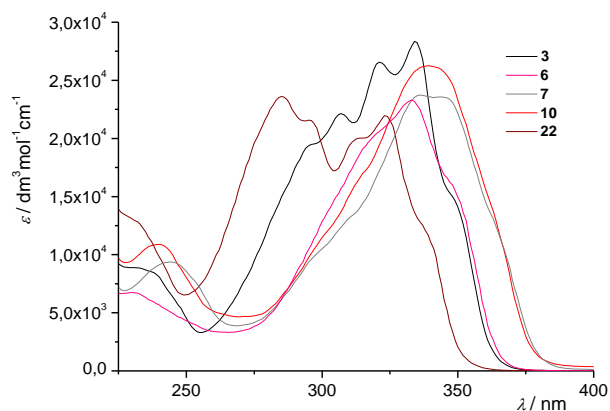
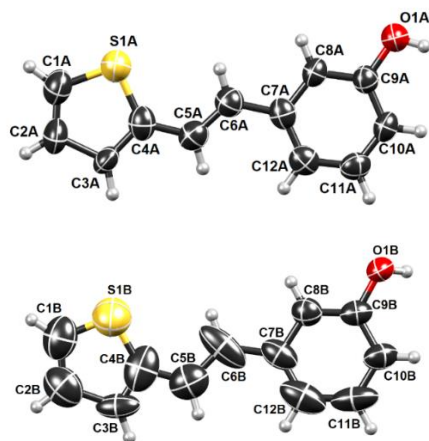


Figure 5. UV spectra in acetonitrile of new compounds **3**, **6**, **7**, **10**, and **22**.

2.2. Crystal structures of **5** and **14**

Compounds **5** and **14** were crystallized, and their crystal structures have been determined. The asymmetric unit of **5** comprises three molecules ($Z'=3$) labeled A, B, and C (Figure 6). A single proton donor is the OH group, which also acts as a proton acceptor. Three symmetry-independent hydrogen bonds link the molecules into chains parallel to [001], and the molecules in them are arranged in the sequence ...ACB... (Figure 7). The asymmetric unit of **14** comprises one molecule (Figure 8), which links it to its symmetry equivalent by a single O-H...O hydrogen bond (Table S3). Thus are formed zigzag chains parallel to [100] (Figure 9). There are only dispersion interactions between the chains.



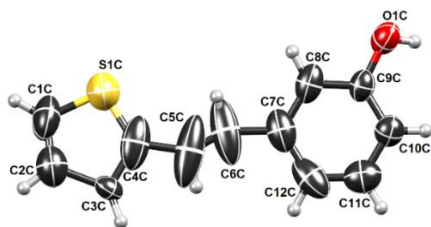


Figure 6. Drawing of three symmetry-independent molecules in **5**, with atom numbering scheme. Displacement ellipsoids are shown for the probability of 50 %, and hydrogen atoms are shown as spheres of arbitrary radii.

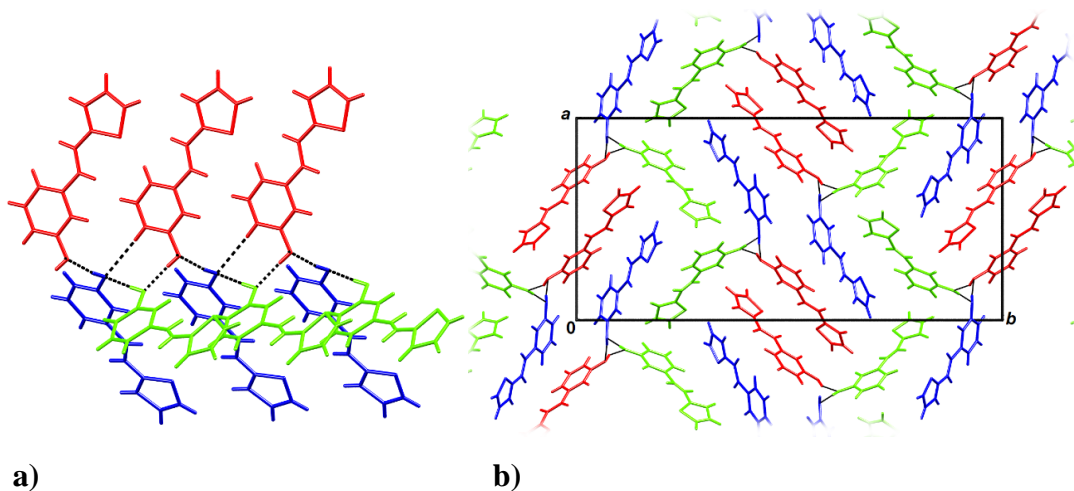


Figure 7. Crystal packing of **5**: a) a hydrogen-bonded chain and b) packing of chains viewed in the direction [001]. Molecule A is shown as red, molecule B is blue, and molecule C is green.

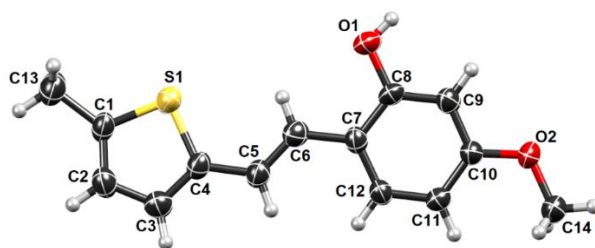


Figure 8. Drawing of molecules of **14** with the atom numbering scheme. Displacement ellipsoids are shown for the probability of 50 %, and hydrogen atoms are shown as spheres of arbitrary radii.

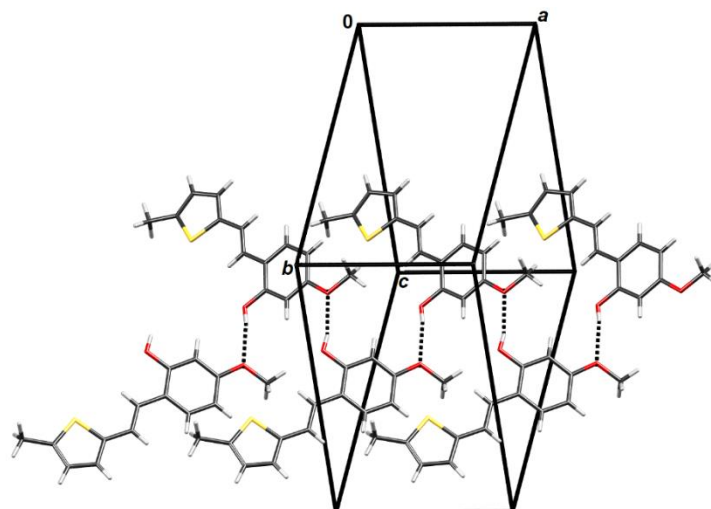


Figure 9. A hydrogen-bonded chain in crystal packing of **14**.

2.3. Antioxidative activity and cholinesterase inhibition of novel resveratrol derivatives

All synthesized compounds represent structural modifications of resveratrol so that instead of one phenolic ring, a heterocyclic ring was introduced on the ethylene bridge: thiophene, substituted thiophene, pyranone, **thiazole** or furan. In addition, the position and type of substituent were also modified on the phenolic part.

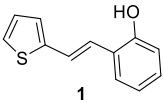
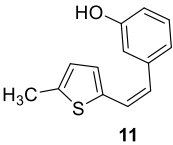
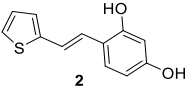
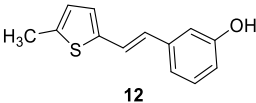
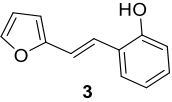
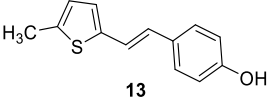
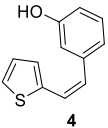
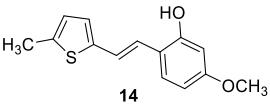
Eighteen stilbene derivatives were assessed for antioxidant activity (AOA) by two methods (DPPH and CUPRAC assay) and acetylcholinesterase (AChE) and butyrylcholinesterase (BChE) inhibition potency.

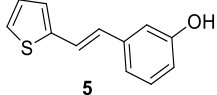
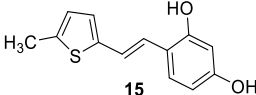
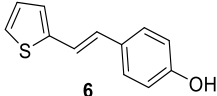
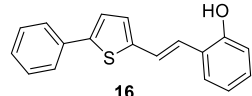
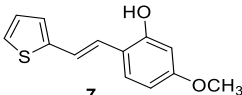
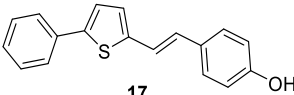
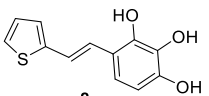
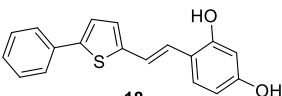
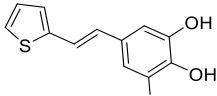
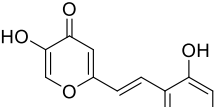
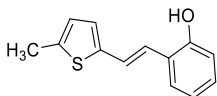
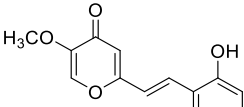
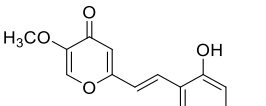
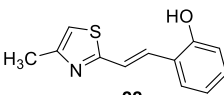
Previously studied compounds **1** and **2** showed good and excellent AOA, respectively, so exploring further derivatization of the core unit appeared promising. The results of the antioxidant study revealed a few new potent antioxidants. In the DPPH assay, a decrease in absorbance of DPPH radical is monitored in the presence of tested compounds. If more than 50% of radical quenching is achieved, the compound concentration necessary for half-maximal reduction (IC_{50}) is calculated (**Table 1**). The furan ring in derivative **3** suits the most for antioxidant reaction, but thiophene and methylated thiophene derivatives also showed strong activity. The most active thiophenes were two substituted derivatives **7** and **14**, with the only difference between them being the presence of methyl at the thiophene ring. The *ortho*-OH and *para*-OCH₃ are shown to be the most reactive in

antioxidant reactions. Replacement of hydrogen from the *para*-OH group in derivative **2** to the methyl group in derivative **7** preserved the AOA in the same range. However, the same substitution had a different effect in structures **14** and **15**, where derivative **15** with two hydroxyl groups showed no AOA while **14** was an excellent antioxidant. Most of the monosubstituted phenolic derivatives showed great to quite good AOA in the following order: **10** > **5** > **4** > **12** > **6** > **13**. Three OH groups, in any arrangement, do not allow involvement in antioxidant reaction since **8** and **9** showed no AOA. The phenolic part of the molecule seems completely inactive for antioxidant reactions when it is connected to pyranone and thiophene with a phenyl ring, regardless of the number and position of OH groups. Generally, the AOA of polyphenolic compounds depends on the redox properties of the hydroxyl group and the potential for electronic delocalization [32]. The number and position of OH groups and the type of heterocycle present affect the effectiveness of AO. Besides that, the overall 3D structure can affect AOA.

In the Cuprac test, the absorbance of the chromophore resulting from the redox reaction of the tested antioxidant with the Cuprac reagent is recorded. Results are expressed as a mole of Trolox per mole of synthesized compound. The Cuprac test confirmed the results of the DPPH assay, and maximum antioxidant capacity was observed for **3**, **5**, **7**, **10**, and **14**.

Table 1. Antioxidant activity values to DPPH method and CUPRAC method of synthesized compound.

Compound	DPPH IC ₅₀ (μM)	Cuprac mol TE/mol of compound	Compound	DPPH IC ₅₀ (μM)	Cuprac mol TE/mol of compound
	158.0**	n.d.		-	0.1128
	26.8**	n.d.		126.8	0.5640
	0.51	1.015		416.3	0.7540
	101.0	0.6731		28.6	1.0029

	82.3	0.7503		-	0.1491
	152.0	0.2292		-	-
	16.4	1.0022		-	-
	-	0.0040		-	-
	-	0.0040		251.3*	n.d.
	45.7	0.7806		-	-
Resveratrol	74.0 [33]	-		-	-
				-	-

*[27]; **[28];

To determine the biological potency of synthesized stilbenes as AChE and BChE inhibitors by the Ellman [34] modified method, compounds were tested in a wide range of concentrations, and if inhibition was higher than 50% the IC₅₀ value was calculated (Table 2). Concerning all the biological evaluation results, it is clear that the strongest antioxidants also **show the best potential toward enzyme BChE**. The matching of multiple biological actions makes these derivatives interesting multi-target drug candidates. Most of the tested thiophenes displayed inhibitory activity, preferably to BChE rather than AChE. Entirely selective inhibitors were **7, 10, and 15**, among which **10** was the most potent **inhibitor toward BChE with** an IC₅₀ value better than the reference

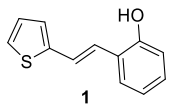
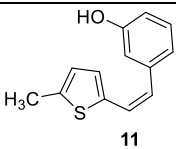
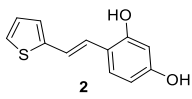
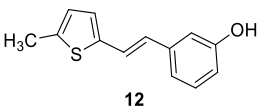
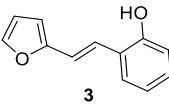
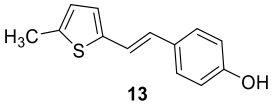
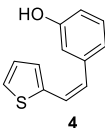
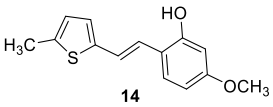
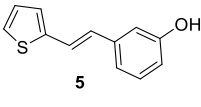
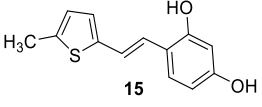
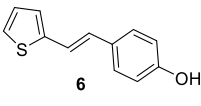
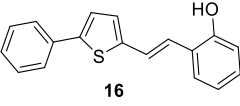
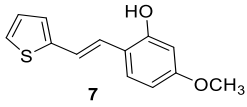
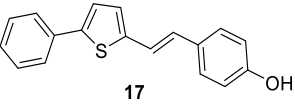
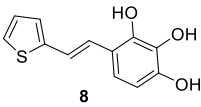
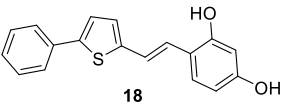
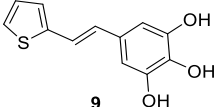
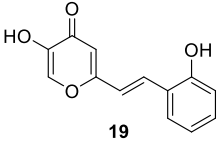
galantamine. **Compounds 3, 12, and 14 inhibited both enzymes and achieved the best IC₅₀ values.** When the *p*-hydroxy group in structure **15** is substituted with the *p*-methoxy (compound **14**), the activity toward AChE occurs, while the activity toward BChE is significantly increased. The introduction of methyl substituent to thiophene in compound **1** (which gave derivative **10**) resulted in the loss of inhibitory activity toward AChE and, at the same time, in the improvement of already good activity toward BChE. Analogous change in compound **6**, which was non-active toward both enzymes, yielded derivative **13**, which showed inhibitory potential toward BChE. Therefore, it seems that, in thiophene analogs of mono-hydroxy resveratrol derivatives, the methylation of thiophene negatively influences the activity toward AChE and, at the same time, leads to better activity toward BChE. The inhibitory activity toward AChE is also lost after the methylation of the thiophene in di-hydroxy resveratrol derivative **2** (compound **15**); however, unexpected activity worsening toward BChE is also observed. When the phenyl substituent is present at thiophene, the impact is much more unambiguous: introducing phenyl to thiophene resulted in a complete loss of all the biological activity tested. Finally, the only compounds not showing AOA but inhibited enzymes were polyhydroxylated **8** and **9**, with three OH groups. However, these results could result from the lack of complete purification after synthesis of **8** and **9** by Wittig reaction, and 10% of triphenylphosphine-oxide remained in tested samples.

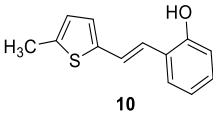
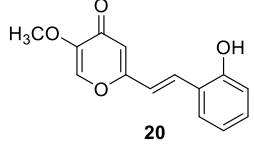
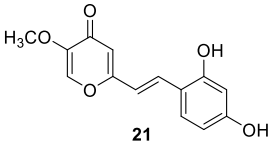
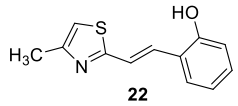
Metoxylated maltol derivatives **20** and **21** did not show any biological activity. When maltol **20** is compared with previously studied (**19**, [27]), it can be seen that replacing the hydroxy group on maltol with a methoxy group completely erases already poor biological activity. The tested furan **3**, a powerful antioxidant, excellently inhibits BChE and **barely** inhibits AChE.

When analyzing all the results of biological studies for derivatives with the same phenol part, for example, **1, 3, 10, 16, and 20**, it is evident that they differ significantly depending on the heterocyclic part of the molecule. The type of heterocycle and its substituent affect biological activity more strongly than the type and position of substituent on a phenolic part.

The thiophene ring is the most favorable for biological activity, while the maltol ring, as a part of the stilbene frame, is completely inactive in selected biological assays.

Table 2. Calculated IC₅₀ values for the inhibition of eeAChE and eqBChE by synthesized compounds

Compound	IC ₅₀ (μM) eeAChE	IC ₅₀ (μM) eqBChE	Compound	IC ₅₀ (μM) eeAChE	IC ₅₀ (μM) eqBChE
	15.7**	4.6**		432.0	575.7
	46.6**	5.3**		51.2	40.9
	482.6	4.7		-	65.0
	194.0	112.0		95.8	4.5
	618.0	116.6		-	129.5
	-	-		-	-
	-	2.4		-	-
	67.4*	6.2*		-	-
	43.4*	3.4*		-***	600.7**

	-	0.8		-	-
Galantamine	0.15	7.9		-	-
				-	25.2

* These results are unreliable since complete purification after synthesis of **8** and **9** by Wittig reaction was not achieved, and 10% of triphenylphosphine-oxide remained in tested samples. ***[27]; **[28]

2.3. Computational study

Compound **10**, a resveratrol derivative featuring a methylated thiophene subunit, displayed remarkably potent inhibitory activity against BChE. We conducted a molecular docking study to identify potential interactions responsible for the stability of the reversible complex formed by this ligand with the enzyme. Figure 10 illustrates the structure of the most stable complex achieved through docking between the active site of BChE and molecule **10**.

The presence of a hydroxy group in the resveratrol derivatives allows for the formation of hydrogen bond(s) with residues within the active site. In this ligand orientation of **10**, the hydroxyl group's proton is positioned near the ϵ -nitrogen of His438 within the esteratic site, thus forming one H-bond. The ligand's phenyl core is involved in π - π stacking with Phe329, while being engaged in a π -alkyl stabilizing interaction with Leu286 within the acyl pocket. The double CC bond of the ligand engages in a similar contact with one of the glycine residues in the oxyanion hole, specifically Gly116. Finally, the thiophene ring is positioned near Trp82, facilitating an alkyl- π contact between the methyl substituent on the thiophene and Trp82.

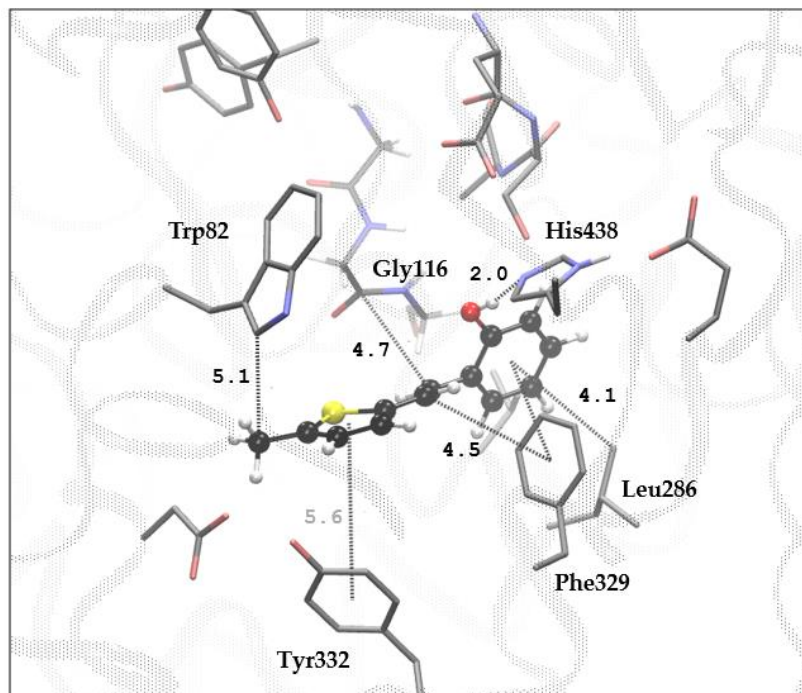


Figure 10. The structure of the BChE's active site docked with compound **10**. Distances given in angstroms, hydrogen atoms of the residues omitted for clarity.

To assess the stability of the ligand-enzyme complex resulting from molecular docking, we conducted a molecular dynamics study (MD) with a production simulation duration of 100 ns. Analysis of the MD results commenced with the calculation of root-mean-square deviation (RMSD) values for all atoms within the complex, excluding hydrogens. The RMSD values for the **10**-BChE complex, reflecting structural changes during the simulation, are depicted in Figure 11.

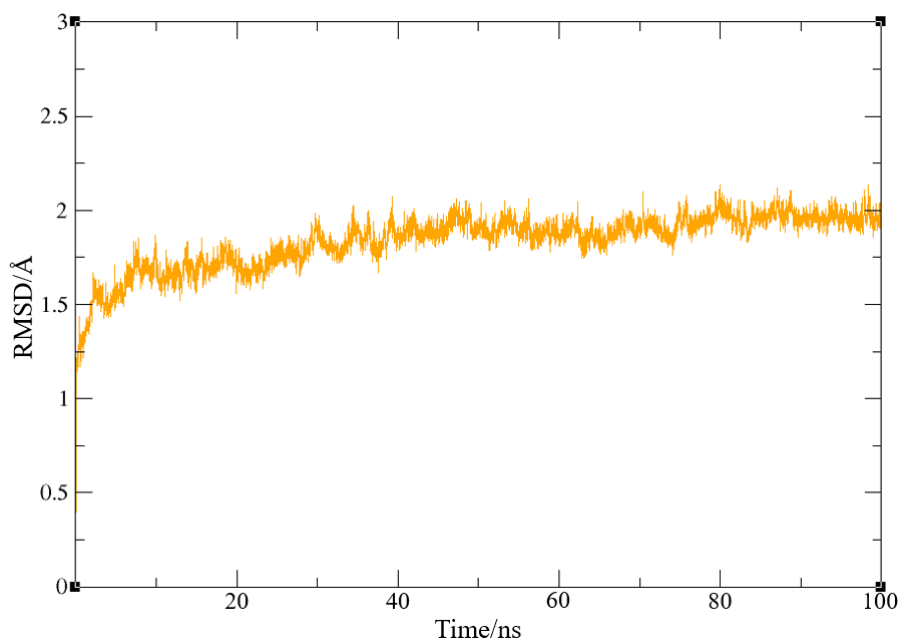


Figure 11. Root-mean-square deviation values from molecular dynamics simulation of a protein-ligand complex of BChE with compound **10**.

Throughout the entire simulation, RMSD values ranged from 0.79 to 2.14 Å, with an average of 1.84 Å. Figure 11 illustrates that the system achieves convergence after 30 ns, with the average RMSD for the last 70 ns decreasing to 1.58 Å, and minimum and maximum values reducing to 0.70 and 1.99 Å, respectively. Root-mean-square fluctuations (RMSF), shown in Figure 12(a), are calculated as the average quadratic fluctuations in the positions of α carbons over the trajectory, identifying the most mobile regions of the protein backbone. Additionally, the radius of gyration (Rg), representing a measure of complex compactness, was computed as the root-mean-square average of the distance of all atoms from the center of mass of the protein-ligand complex and is presented in Figure 12(b). Systems where Rg remains relatively stable throughout the simulation are described as compact.

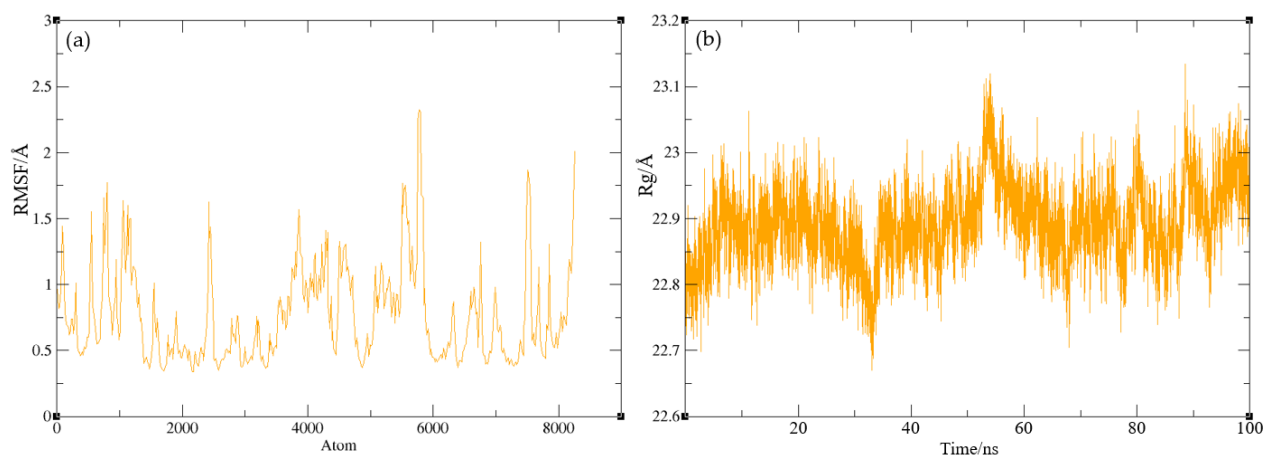


Figure 12. (a) Root-mean-square fluctuation values from molecular dynamics simulation of a protein-ligand complex of BChE with compound **10**, and (b) radius of gyration plot for the same complex.

RMSF values spanned from 0.34 to 2.33 Å, with an average value of 0.77 Å, indicating that positions of α carbons in the backbone exhibited limited fluctuations during the simulation. The close analysis of the plot presented in Figure 12(a) reveals that α -carbon with the highest RMSF value (2.33 Å) is indexed as 5777, belonging to Val374. The plot presented in Figure 12(b) shows that changes in the radius of gyration were minor, with this parameter varying within the range of 22.67 to 23.13 Å.

Among new resveratrols, the only derivative with a furan ring, compound **3**, showed auspicious inhibitory activity towards BChE. The most stable orientation of the ligand obtained by the docking of **3** into the site of BChE is shown in Figure 13. Just as in the complex of BChE with resveratrol derivative **10**, one H-bond is observed; here, hydrogen from the hydroxyl group of the ligand interacts with Asp70, a residue belonging to the peripheral anionic site (PAS). The phenyl ring is placed at a distance of 6 Å from Trp82, resulting in T-shaped π - π stacking. Among the newly studied resveratrol derivatives, compound **3**, featuring a furan ring, exhibited promising inhibitory activity against BChE, although, unlike compound **10**, it is not selective. Figure 13 showcases the most stable orientation of the ligand as obtained through docking into the BChE site. Like in the **10**-BChE complex, one hydrogen bond is observed, with hydrogen from the ligand's hydroxyl group forming an H-bond with Asp70, a residue in the peripheral anionic site. The phenyl ring is approximately 6 Å away from Trp82, leading to T-shaped π - π stacking.

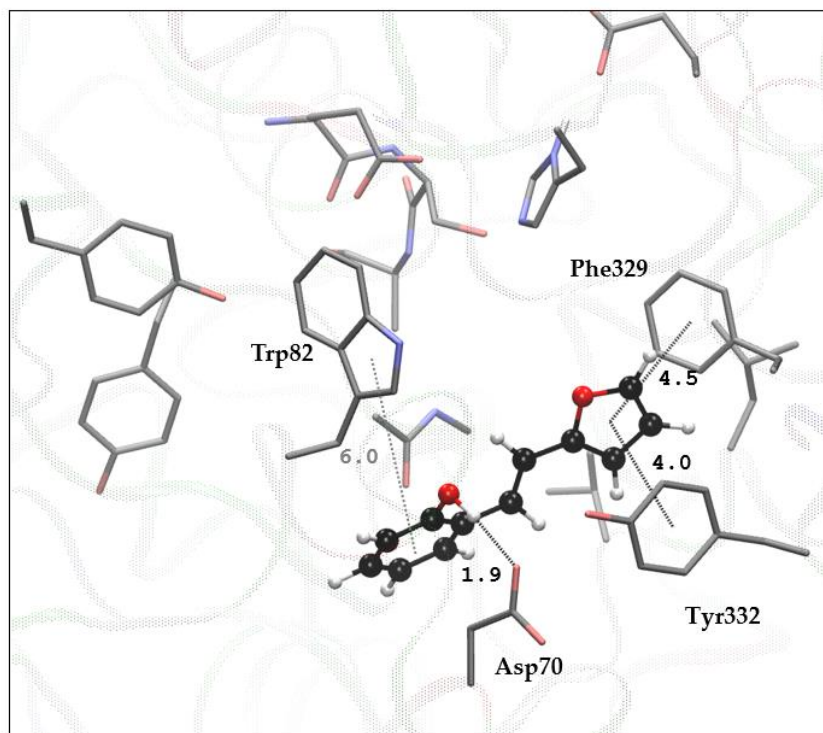


Figure 13. The structure of the BChE's active site docked with compound **3**. Distances given in angstroms, hydrogen atoms of the residues omitted for clarity.

The furan ring also engages in π - π stacking interactions, this time with Phe329 and Tyr332 on the opposite side of furan's plane. However, this orientation of ligand **3** does not involve contact with the acyl pocket and is situated too far from the esteratic site.

To assess the stability of the ligand-protein complex, we conducted a 100 ns molecular dynamics simulation, monitoring also α -carbon fluctuations and the protein's compactness. Figure 14 displays the RMSD values throughout the simulation, which ranged from 0.78 to 2.46 Å, with an average value of 2.09 Å. This result is slightly less favorable than the **10**-BChE ligand-protein complex, but it still confirms the overall stability of the complex.

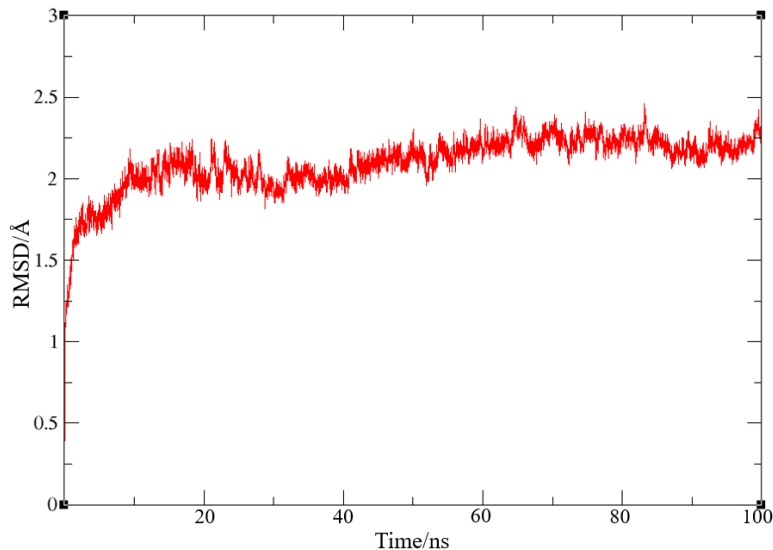


Figure 14. Root-mean-square deviation values from molecular dynamics simulation of a protein-ligand complex of BChE with compound **3**.

Similarly to the previously analyzed system, full convergence was achieved after 30 ns, resulting in an average RMSD of 1.93 Å for the last 70 ns (with minimum and maximum values of 0.75 and 2.34 Å).

Lastly, we calculated RMSF values for α carbons and the radius of gyration for the system involving compound **3**, with results presented in Figure 15(a) and (b). Here, RMSF values were slightly higher than the system with molecule **3**, with an average RMSF of 0.78 Å. Notably, the maximum α -carbon fluctuation value (2.44 Å) was observed for residue Val374, mirroring the case of the system with compound **3** where this value was 2.33 Å.

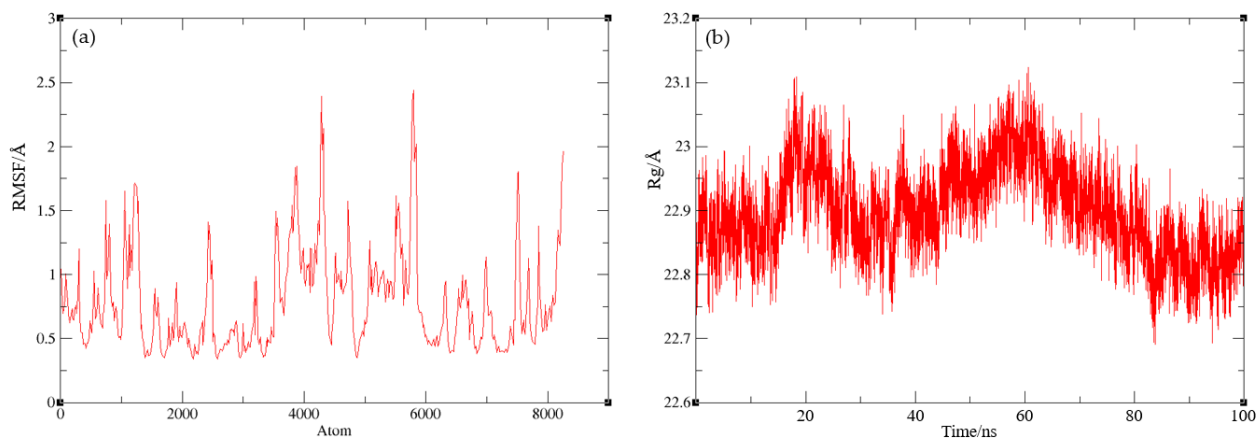


Figure 15. (a) Root-mean-square fluctuation values from molecular dynamics simulation of a protein-ligand complex of BChE with compound **3**, and (b) radius of gyration plot for the same complex.

Additionally, the radius of gyration values indicated that the protein's compactness was preserved during the simulation, with Rg values falling within a narrow range of 22.79 to 23.12 Å.

2.4. Genotoxicity - ICH (M7) Q(SAR)

In the process of pharmaceutical development, it is crucial to identify and, as much as possible, isolate or synthesize all impurities that could be present in the active pharmaceutical compound (API) or the drug product. All impurities potentially present in the API and each intermediate in the manufacturing process must also be evaluated, at least with the *in silico* models.

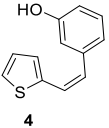
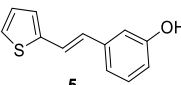
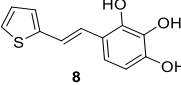
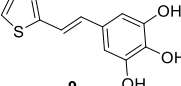
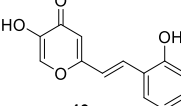
Within the scope of impurities of drug substances and drug products, there is a special category: the possible mutagenic/carcinogenic impurities. They are more strictly regulated and must be controlled at much lower limits than all other impurities. The regulation that is followed for this kind of compounds is the ICH M7 Guideline. The levels that can be present in the drug substance or the drug product have to be calculated individually for each identified PMI (possible mutagenic compound) based on their determined acceptable daily intake (ADI) and the maximum daily dose of the drug (MDD) that the patient can take. Suppose toxicological studies on animals have not determined the ADI. In that case, the most conservative approach must be taken with the most strict presumed ADI described in the guideline.

It is common with the development of new drug substances and drug products that the impurities that appear will also be new compounds, and there will be no experimental data available for them in the literature databases. In these cases, the Q(SAR) approach is vital. (Q)SAR models predict biological activity based on structural components [35]. This approach for evaluating the mutagenic potential of compounds can also be used to determine the mutagenic potential during the early stages of searching for potentially active drug substances. This will help by eliminating all compounds with biological activity but also mutagenic potential. The most commonly used tool is the Lhasa software because it consists of two complementary models (one rule-based and the other statistical-based); their predictions are then reviewed one more time by an expert.

In the case of compounds **1-22** that are investigated for their potential biological activity with the emphasis on inhibiting enzymes cholinesterases (ChEs) and antioxidative activity, **of all tested structures**, only five structures were identified by the software to have a potential for mutagenicity

(Table 3), not being the most active derivatives in terms of both ChE and antioxidant activities, which further enhances the best biological results.

Table 3. Compounds with a positive mutagenic potential by Lhasa M7 evaluation.

Structure	ICH M7 Class	Cohort of Concern	Derek Prediction	Sarah Prediction	Exp. Data	Similarity to API	Overall In Silico
 4	Class 3	No	■ ■ ■ □	■ □ □ □	Carc: Unspecified Ames: Unspecified	No Derek Alerts were found	Positive
 5	Class 3	No	■ ■ ■ □	■ □ □ □	Carc: Unspecified Ames: Unspecified	No Derek Alerts were found	Positive
 8	Class 3	No	■ ■ ■ □	□ □ □ □	Carc: Unspecified Ames: Unspecified	Alert(s) not found in API	Positive
 9	Class 3	No	■ ■ ■ □	□ □ □ □	Carc: Unspecified Ames: Unspecified	Alert(s) not found in API	Positive
 19	Class 3	No	■ □ □ □	□ □ □ □	Carc: Unspecified Ames: Unspecified	Alert(s) not found in API	Positive

Two of these structures were identified based on Sarah predictions. Sarah is a rule-based model, meaning that it was trained by an algorithm. Compounds **8**, **9**, and **19** are positive based on the Derek predictions (expert-based models trained by expert inputs and real-time data obtained from the literature). For compounds **4** and **5**, the moieties that Sarah considers possibly positive are thiophene and hydroxybenzenes; however, Derek is not finding any hits in its database. If they were to be shown as highly biologically active, an experimental AMES test could be then performed on mutated cell assays to determine whether the mutagenic potential is real. The compounds **8**, **9**, and **19**, which are found in the Derek database and have a trihydroxybenzene moiety, are probably mutagenic, and the investigation into their further activity as drug substances should be stopped, as this moiety is already known and considered to be potentially mutagenic [36].

3. Materials and Methods

3.1. General remarks

The following solvents and chemicals were used in the experiments: acetone, acetonitrile - ACN, boron tribromide - BBr₃, diethyl ether - E, dichloromethane - DCM, ethanol - EtOH, ethyl acetate - EtOAc, potassium hydroxide - KOH, chloroform - CHCl₃, sodium hydroxide - NaOH, sodium hydrogen carbonate - NaHCO₃, methanol - MeOH, petroleum ether - PE, carbon tetrachloromethane - CCl₄, and toluene. All solvents used were purified by distillation and are commercially available. Reagents such as 2,2-azobis(2-methylpropionitrile) (AIBN), dimethylsulfate ((CH₃)₂SO₄), *N*-bromosuccinimide (NBS), and thionyl chloride (SOCl₂) were used in the synthesis. To synthesize phosphonium salts, triphenylphosphine (PPh₃) was used as a purchased chemical. In Wittig's reactions, sodium (Na) stored in PE was used, which reacted with EtOH to give sodium ethoxide (NaOEt). Anhydrous MgSO₄ was used to dry the organic layer after extraction. To perform thin-layer chromatography (TLC), plates coated with silica gel (0.2 mm, Kieselgel 60 F₂₅₄) were used. When performing column chromatography, columns filled with silica gel (60 Å, technical) were used, and solvents were evaporated using a rotary evaporator under reduced pressure.

¹H and ¹³C NMR spectra were recorded on a Bruker Avance spectrometer operating at a frequency of 600 MHz for ¹H nuclei and a frequency of 150 MHz for ¹³C nuclei. Deuterated chloroform - CDCl₃ and deuterated methanol - CD₃OD were used to dissolve compounds, and tetramethylsilane - TMS was used as a standard for recording NMR spectra. Chemical shifts are expressed in ppm (parts per million), and the following symbols were used to characterize the signal: s – singlet, d – doublet, dd – doublet of doublets, t – triplet, and m – multiplet. UV spectra were recorded on a UV/Vid spectrophotometer, and ACN was used as a solvent for the compounds. HRMS analyses to confirm the samples' purity were carried out in collaboration with PLIVA on a mass spectrometer (MALDI TOF/TOF analyzer) equipped with a Nd:YAG laser operating at 355 nm with an adjustment speed of 200 Hz.

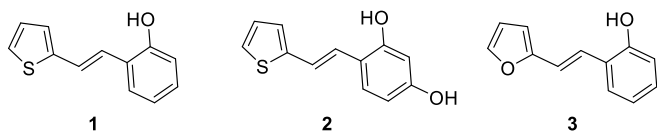
3.2. Synthesis of furan and thiophene phosphonium salts

Synthesis of bromo(4-methoxybenzyl)triphenyl- λ^5 -phosphane, bromo(furan-2-yl-methyl)triphenyl- λ^5 -phosphane, bromo(thiophen-2-yl-methyl)triphenyl- λ^5 -phosphane and bromo((5-methylthiophen-2-yl)methyl)triphenyl- λ^5 -phosphane was carried out in round flasks (0.5 L) by preparing the corresponding furan and thiophene bromides using AIBN and NBS reagents. To a solution of 4-methoxytoluene, 2-methylfuran, 2-methylthiophene, or 2,5-dimethylthiophene (100.0 mmol) in CCl_4 (0.05 mL) was added NBS (110.0 mmol) and AIBN (1.28 mmol). The reaction mixture in the flask was then heated to reflux using a chlor-calcium tube condenser at the reflux temperature of CCl_4 using an oil bath. After two hours of reflux, the resulting succinimide was filtered into a round flask (0.25 mL), CCl_4 evaporated, and a light brown bromide oil remained. PPh_3 (100.0 mmol) previously dissolved in toluene (0.08 mL) was added to the obtained bromide in a flask, and the mixture was stirred at room temperature for 40 hours. Vacuum filtration was carried out using a Büchner funnel, after which the salt was dried in a desiccator under vacuum for six hours and then left in the desiccator for three days. The dry salt was further used to synthesize the desired compounds by different synthetic routes.

3.3. Synthesis of new resveratrol derivatives **1-15**

Compounds **1-15** were synthesized as cis- and trans-isomers mixtures by the Wittig reaction. Before carrying out the reaction, the apparatus was blown with nitrogen for 15 minutes. The reaction was carried out in a three-necked flask (250 mL), on the two side necks of which a chlor-calcium tube and a balloon with N_2 were placed, connected via a needle and a septum to the neck of the flask. A dropping funnel was attached to the middle neck of the flask, into which 50 mL of EtOH was added, and half the volume was dropped into the flask. The appropriate phosphonium salt (2.2 – 4.7 mmol) was then added to the flask, stirring the mixture using a magnetic stirrer. Weighed Na (1.1 eq) was added gradually over 20 minutes to the remaining 25 mL of EtOH. The mixture was allowed to stir until all the Na had reacted to NaOEt. Then, aldehyde (1 eq) was added to the reaction mixture with NaOEt added dropwise, and the reaction mixture was left to stir for a certain time (**1-14** – 72 h, **15** – 168 h) at a certain temperature (**1-9**, **11-14** – 25 °C, **10**, **15** – 100 °C). The reaction mixture was evaporated on a rotary evaporator under reduced pressure and dissolved in toluene (**1-5**, **10-14**) or CHCl_3 (**6-9** and **15**). The mixture was then extracted with toluene (**1-5**, **10-14**) or CHCl_3 (**6-9** and **15**) (3 x 15 mL), depending on the solubility of the product. The organic layer was separated in an Erlenmayer flask and dried over MgSO_4 , a drying agent.

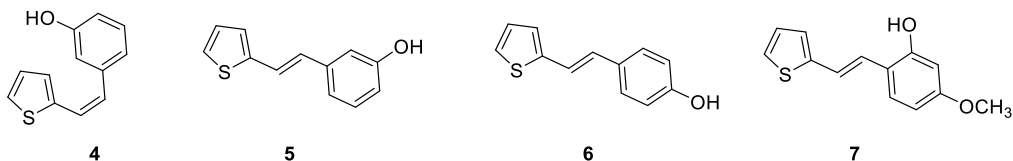
After 30 minutes of drying, the solvent was evaporated, and the organic product as a mixture of isomers (with different proportions of *cis*-isomers) was purified on a column filled with silica gel. Pure *trans*-isomers are isolated by sequential column chromatography or thin-layer chromatography. PE/E and PE/EtOAc solvent systems of different polarities were used as eluents.



(*E*)-2-(2-(Thiophen-2-yl)vinyl)phenol (**1**) [28]: 495 mg, 82% isolated; white powder, m. p. 126–127 °C; R_f (PE/DCM (50 %)) = 0.33; UV (ACN) λ_{max}/nm ($\epsilon/dm^3mol^{-1}cm^{-1}$) 335 (27412); 1H NMR ($CDCl_3$, 600 MHz) δ/ppm : 7.46 (dd, $J = 7.7, 1.6$ Hz, 1H), 7.28 (dt, $J = 16.1, 0.8$ Hz, 1H), 7.20 – 7.16 (m, 2H), 7.15 – 7.10 (m, 1H), 7.07 (dt, $J = 3.7, 0.9$ Hz, 1H), 6.99 (dd, $J = 5.1, 3.5$ Hz, 1H), 6.93 (td, $J = 7.5, 1.2$ Hz, 1H), 6.78 (dd, $J = 8.1, 1.2$ Hz, 1H), 4.97 (s, 1H); ^{13}C NMR ($CDCl_3$, 150 MHz) δ/ppm : 152.9, 143.3, 128.6, 127.6, 127.2, 126.0, 124.4, 124.3, 123.3, 122.7, 121.2, 115.9; MS (ESI) (m/z) (% , fragment): 202 (25), 105 (100).

(*E*)-4-(2-(Thiophen-2-yl)vinyl)benzene-1,3-diol (**2**) [28]: 79 mg, 51% isolated; white powder, m. p. 141–143 °C; R_f (PE/E (50 %)) = 0.16; UV (ACN) λ_{max}/nm ($\epsilon/dm^3mol^{-1}cm^{-1}$) 343 (28311), 336 (28462); 1H NMR ($CDCl_3$, 600 MHz) δ/ppm : 7.33 – 7.30 (m, 1H), 7.17 – 7.12 (m, 2H), 7.05 (d, $J = 16.2$ Hz, 1H), 7.03 (dt, $J = 3.6, 1.0$ Hz, 1H), 6.99 (dd, $J = 5.1, 3.5$ Hz, 1H), 6.42 (dd, $J = 8.4, 2.4$ Hz, 1H), 6.33 (d, $J = 2.5$ Hz, 1H), 5.02 (s, 1H), 4.78 (s, 1H); ^{13}C NMR ($CDCl_3$, 150 MHz) δ/ppm : 156.1, 154.1, 143.5, 128.4, 127.5, 125.4, 123.9, 122.5, 121.6, 117.5, 108.6, 103.2; MS (ESI) (m/z) (% , fragment): 241 ($M^+ + Na$, 10), 218 (5), 201 (100).

(*E*)-2-(2-(Furan-2-yl)vinyl)phenol (**3**): 250 mg, 28% isolated; yellow powder; m. p. 78–82 °C; R_f (PE/E (30 %)) = 0.43; UV (ACN) λ_{max}/nm ($\epsilon/dm^3mol^{-1}cm^{-1}$) 334 (28358), 321 (26567), 307 (22128), 297 (sh, 19523); 1H NMR ($CDCl_3$, 300 MHz) δ/ppm : 7.46 – 7.40 (m, 2H), 7.28 – 7.22 (m, 1H), 7.13 (t, $J = 7.8$ Hz, 1H), 6.99 – 6.91 (m, 2H), 6.79 (d, $J = 7.9$ Hz, 1H), 6.43 – 6.41 (m, 1H), 6.35 (d, $J = 3.6$ Hz, 1H), 4.96 (s, 1H); ^{13}C NMR ($CDCl_3$, 150 MHz) δ/ppm : 153.5, 153.1, 142.1, 128.6, 127.3, 124.3, 121.6, 121.2, 118.1, 116.0, 111.6, 108.5; MS (ESI) (m/z) (% , fragment): 187 (100), 121 (15); HRMS (m/z) for $C_{12}H_{10}O_2$: $[M+H]^+$ calculated = 186.0681, $[M+H]^+$ measured = 186.0683.

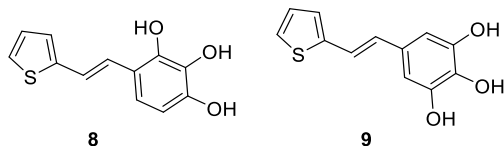


(*Z*)-3-(2-(Thiophen-2-yl)vinyl)phenol (**4**): 190 mg, 40% isolated; colorless oil; R_f (PE/E (20 %)) = 0.25; $^1\text{H NMR}$ (CDCl_3 , 600 MHz) δ /ppm: 7.24 – 7.21 (m, 1H), 7.09 (d, $J = 5.0$ Hz, 1H), 6.97 (d, $J = 3.3$ Hz, 1H), 6.92 (d, $J = 7.8$ Hz, 1H), 6.88 (dd, $J = 4.8, 3.6$ Hz, 1H), 6.83 (s, 1H), 6.77 (dd, $J = 8.0, 2.5$ Hz, 1H), 6.68 (d, $J = 12.3$ Hz, 1H), 6.51 (d, $J = 12.3$ Hz, 1H), 4.81 (s, 1H); $^{13}\text{C NMR}$ (CDCl_3 , 150 MHz) δ /ppm: 155.6, 139.6, 138.9, 129.9, 128.3, 126.5, 125.7, 123.6, 121.4, 115.5, 114.5.

(*E*)-3-(2-(Thiophen-2-yl)vinyl)phenol (**5**): 13 mg, 5% isolated; white powder; R_f (PE/E (18 %)) = 0.24; $^1\text{H NMR}$ (CDCl_3 , 600 MHz) δ /ppm: 7.22 – 7.18 (m, 3H), 7.06 (d, $J = 3.9$ Hz, 1H), 7.04 (d, $J = 7.9$ Hz, 1H), 7.00 (dd, $J = 5.4, 3.3$ Hz, 1H), 6.94 (t, $J = 2.1$ Hz, 1H), 6.86 (d, $J = 15.9$ Hz, 1H), 6.72 (dd, $J = 7.9, 2.5$ Hz, 1H), **4.78 (s, 1H)**; $^{13}\text{C NMR}$ (CDCl_3 , 150 MHz) δ /ppm: 155.8, 142.7, 138.7, 129.9, 127.8, 127.6, 126.3, 124.5, 122.3, 119.3, 114.7, 112.7; MS (ESI) (m/z) (% , fragment): 203 (100); HRMS (m/z) for $\text{C}_{12}\text{H}_{10}\text{OS}$: $[\text{M}+\text{H}]^+$ calculated = 202.0452, $[\text{M}+\text{H}]^+$ measured = 202.0458.

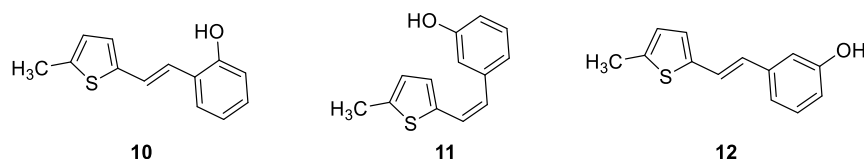
(*E*)-4-(2-(Thiophen-2-yl)vinyl)phenol (**6**): 10 mg, 3% isolated; yellow powder; m. p. 123-124 °C; R_f (PE/DCM (40 %)) = 0.17; UV (ACN) $\lambda_{\text{max}}/\text{nm}$ ($\epsilon/\text{dm}^3\text{mol}^{-1}\text{cm}^{-1}$) 333 (23297); $^1\text{H NMR}$ (CDCl_3 , 600 MHz) δ /ppm: 7.35 (d, $J = 8.7$ Hz, 2H), 7.15 (d, $J = 5.6$ Hz, 1H), 7.09 (d, $J = 16.2$ Hz, 1H), 7.02 (d, $J = 3.4$ Hz, 1H), 6.99 – 6.98 (m, 1H), 6.87 (d, $J = 16.2$ Hz, 1H), 6.81 (d, $J = 8.5$ Hz, 2H), 4.93 (s, 1H); $^{13}\text{C NMR}$ (CDCl_3 , 75 MHz) δ /ppm: 155.8, 143.2, 129.9, 127.9, 127.7, 127.5, 125.4, 123.8, 119.8, 115.6; MS (ESI) (m/z) (% , fragment): 203 (100), 140 (70); HRMS (m/z) for $\text{C}_{12}\text{H}_{10}\text{OS}$: $[\text{M}+\text{H}]^+$ calculated = 202.0452, $[\text{M}+\text{H}]^+$ measured = 202.0448.

(*E*)-5-Methoxy-2-(2-(thiophen-2-yl)vinyl)phenol (**7**): 60 mg, 40% isolated; yellow powder; m. p. 91-94 °C; R_f (PE/E (60 %)) = 0.35; UV (ACN) $\lambda_{\text{max}}/\text{nm}$ ($\epsilon/\text{dm}^3\text{mol}^{-1}\text{cm}^{-1}$) 336 (23732), 244 (9367), 211 (15320); $^1\text{H NMR}$ (CDCl_3 , 600 MHz) δ /ppm: 7.36 (d, $J = 8.7$ Hz, 1H), 7.17 – 7.14 (m, 2H), 7.06 (d, $J = 16.2$ Hz, 1H), 7.03 (d, $J = 3.4$ Hz, 1H), 6.98 (dd, $J = 4.9, 3.7$ Hz, 1H), 6.51 (dd, $J = 8.5, 2.6$ Hz, 1H), 6.37 (d, $J = 2.6$ Hz, 1H), 5.03 (s, 1H), 3.79 (s, 3H); $^{13}\text{C NMR}$ (CDCl_3 , 150 MHz) δ /ppm: 160.2, 153.9, 143.6, 128.2, 127.2, 125.4, 123.8, 122.6, 121.5, 117.3, 107.1, 101.9, 55.4; MS (ESI) (m/z) (% , fragment): 233 (100); HRMS (m/z) for $\text{C}_{13}\text{H}_{12}\text{O}_2\text{S}$: $[\text{M}+\text{H}]^+$ calculated = 232.0558, $[\text{M}+\text{H}]^+$ measured = 232.0556.



(*E*)-4-(2-(Thiophen-2-yl)vinyl)benzene-1,2,3-triol (**8**): 100 mg, with 10% of phosphine oxide; R_f (EtOAc/MeOH (10 %)) = 0.56; $^1\text{H NMR}$ (CDCl_3 , 300 MHz) δ /ppm: 7.81 – 7.74 (m, 2H), 7.68 – 7.62 (m, 2H), 7.18 (t, $J = 3.2$ Hz, 1H), 7.14 – 7.11 (m, 1H), 6.86 (t, $J = 4.2$ Hz, 1H), 5.81 (s, 1H), 5.77 (s, 1H); MS (ESI) (m/z) (% , fragment): 235 (100).

(*E*)-5-(2-(Thiophen-2-yl)vinyl)benzene-1,2,3-triol (**9**): 80 mg, with 10% of phosphine oxide; R_f (EtOAc/MeOH (10 %)) = 0,56; $^1\text{H NMR}$ (CDCl_3 , 300 MHz) δ /ppm: 7.80 – 7.74 (m, 2H), 7.65 – 7.61 (m, 2H), 7.18 (t, $J = 3.5$ Hz, 1H), 7.14 – 7.11 (m, 1H), 6.85 (t, $J = 4.6$ Hz, 1H), 5.81 (s, 1H), 5.76 (s, 1H); MS (ESI) (m/z) (% , fragment): 235 (100).

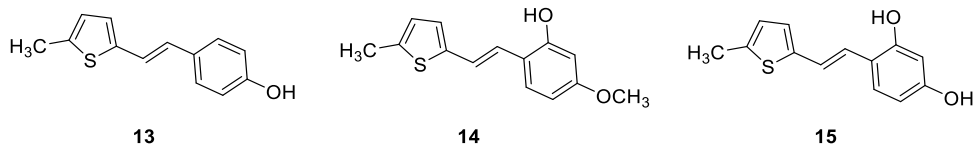


(*E*)-2-(2-(5-Methylthiophen-2-yl)vinyl)phenol (**10**): 95 mg, 40% isolated; yellow powder; m. p. 88-92 °C; R_f (PE/E (20 %)) = 0.54; UV (ACN) λ_{max} /nm ($\epsilon/\text{dm}^3\text{mol}^{-1}\text{cm}^{-1}$) 339 (26378), 240 (10925), 208 (19311); $^1\text{H NMR}$ (CDCl_3 , 600 MHz) δ /ppm: 7.44 (d, $J = 7.3$ Hz, 1H), 7.18 (d, $J = 16.6$ Hz, 1H), 7.11 (t, $J = 7.9$ Hz, 1H), 7.01 (d, $J = 16.6$ Hz, 1H), 6.92 (t, $J = 7.6$ Hz, 1H), 6.85 (d, $J = 2.9$ Hz, 1H), 6.78 (d, $J = 7.9$ Hz, 1H), 6.64 – 6.64 (m, 1H), 4.93 (s, 1H), 2.48 (s, 3H); $^{13}\text{C NMR}$ (CDCl_3 , 150 MHz) δ /ppm: 152.8, 141.2, 139.3, 128.3, 127.1, 126.3, 125.7, 124.5 123.8, 121.4, 121.2, 115.9, 115.6; MS (ESI) (m/z) (% , fragment): 217 (100); HRMS (m/z) for $\text{C}_{13}\text{H}_{12}\text{OS}$: $[\text{M}+\text{H}]^+$ _{calculated} = 216.0609, $[\text{M}+\text{H}]^+$ _{measured} = 216.0607.

(*Z*)-3-(2-(5-Methylthiophen-2-yl)vinyl)phenol (**11**): 180 mg, 38% isolated; colorless oil; R_f (PE/E (50 %)) = 0.65; $^1\text{H NMR}$ (CDCl_3 , 600 MHz) δ /ppm: 7.24 – 7.21 (m, 1H), 6.93 (d, $J = 7.6$ Hz, 1H), 6.83 (s, 1H), 6.78 – 6.76 (m, 2H), 6.59 (d, $J = 12.2$ Hz, 1H), 6.54 – 6.53 (m, 1H), 6.40 (d, $J = 12.2$ Hz, 1H), 4.85 (s, 1H), 2.35 (s, 3H); $^{13}\text{C NMR}$ (CDCl_3 , 150 MHz) δ /ppm: 155.5, 140.5, 139.2, 137.5, 129.8, 128.8, 126.8, 124.6, 123.9, 121.4, 115.6, 114.4, 15.3.

(*E*)-3-(2-(5-Methylthiophen-2-yl)vinyl)phenol (**12**): 43 mg, 8% isolated; yellow powder; m.p. 75-78 °C; R_f (PE/E (50 %)) = 0.63; $^1\text{H NMR}$ (CDCl_3 , 600 MHz) δ /ppm: 7.19 (t, $J = 7.7$ Hz, 1H), 7.11 (d, $J = 15.9$ Hz, 1H), 7.01 (d, $J = 7.5$ Hz, 1H), 6.91 (t, $J = 2.2$ Hz, 1H), 6.84 (d, $J = 3.4$ Hz, 1H),

6.72 (d, $J = 15.9$ Hz, 1H), 6.70 (dd, $J = 8.1, 2.5$ Hz, 1H), 6.65 – 6.64 (m, 1H), 4.72 (s, 1H), 2.48 (s, 3H); ^{13}C NMR (CDCl_3 , 150 MHz) δ/ppm : 155.8, 140.6, 139.5, 139.0, 129.8, 126.5, 126.4, 125.8, 122.7, 119.1, 114.4, 112.6, 15.6; MS (ESI) (m/z) (% , fragment): 168 (100); HRMS (m/z) for $\text{C}_{13}\text{H}_{12}\text{OS}$: $[\text{M}+\text{H}]^+$ _{calculated} = 216.0609, $[\text{M}+\text{H}]^+$ _{measured} = 216.0607.



(*E*)-4-(2-(5-Methylthiophen-2-yl)vinyl)phenol (**13**): 6 mg, 8% isolated; yellow powder; m.p. 79-81 °C; $R_f(\text{PE/E } (60\%)) = 0.42$; ^1H NMR (CDCl_3 , 600 MHz) δ/ppm : 7.32 (d, $J = 8.3$ Hz, 2H), 6.99 (d, $J = 16.6$ Hz, 1H), 6.82 – 6.79 (m, 3H), 6.73 (d, $J = 16.6$ Hz, 1H), 6.63 – 6.62 (m, 1H), 4.95 (s, 3H); ^{13}C NMR (CDCl_3 , 150 MHz) δ/ppm : 155.1, 141.1, 138.6, 134.1, 130.2, 127.5, 126.6, 125.7, 120.3, 115.6, 15.6; MS (ESI) (m/z) (% , fragment): 215 (100); HRMS (m/z) for $\text{C}_{13}\text{H}_{12}\text{OS}$: $[\text{M}+\text{H}]^+$ _{calculated} = 216.0609, $[\text{M}+\text{H}]^+$ _{measured} = 216.0607.

(*E*)-5-Methoxy-2-(2-(5-methylthiophen-2-yl)vinyl)phenol (**14**): 5 mg, 6% isolated; yellow powder; m.p. 91-95 °C; $R_f(\text{PE/E } (60\%)) = 0.45$; ^1H NMR (CDCl_3 , 600 MHz) δ/ppm : 7.33 (d, $J = 8.4$ Hz, 1H), 7.06 (d, $J = 16.3$ Hz, 1H), 6.91 (d, $J = 16.3$ Hz, 1H), 6.80 (d, $J = 3.4$ Hz, 1H), 6.62 (d, $J = 3.1$ Hz, 1H), 6.50 (dd, $J = 8.7, 2.6$ Hz, 1H), 6.37 (d, $J = 2.5$ Hz, 1H), 5.03 (s, 1H), 3.78 (s, 3H), 2.47 (s, 3H); ^{13}C NMR (CDCl_3 , 150 MHz) δ/ppm : 160.0, 153.9, 141.5, 138.7, 128.0, 125.7, 121.9, 121.3, 117.5, 107.1, 101.9, 55.4, 15.6; MS (ESI) (m/z) (% , fragment): 245 (100); HRMS (m/z) for $\text{C}_{14}\text{H}_{14}\text{O}_2\text{S}$: $[\text{M}+\text{H}]^+$ _{calculated} = 246.0715, $[\text{M}+\text{H}]^+$ _{measured} = 246.0712.

(*E*)-4-(2-(5-Methylthiophen-2-yl)vinyl)benzene-1,3-diol (**15**): 10 mg, 12% isolated; yellow powder; m.p. 149-151 °C; $R_f(\text{PE/E } (30\%)) = 0.43$; UV (ACN) $\lambda_{\text{max}}/\text{nm}$ ($\epsilon/\text{dm}^3\text{mol}^{-1}\text{cm}^{-1}$) 341 (15202); ^1H NMR (CDCl_3 , 600 MHz) δ/ppm : 7.28 (d, $J = 8.6$ Hz, 1H), 7.05 (d, $J = 16.3$ Hz, 1H), 6.91 (d, $J = 16.3$ Hz, 1H), 6.80 (d, $J = 3.5$ Hz, 1H), 6.63 – 6.62 (m, 1H), 6.41 (dd, $J = 8.4, 2.3$ Hz, 1H), 6.33 (d, $J = 2.5$ Hz, 1H), 5.02 (s, 1H), 4.77 (s, 1H), 2.47 (s, 3H); ^{13}C NMR (CDCl_3 , 150 MHz) δ/ppm : 155.9, 153.9, 141.5, 138.8, 128.2, 125.7, 125.6, 122.1, 121.1, 117.7, 108.5, 103.2, 15.6; MS (ESI) (m/z) (% , fragment): 233 (100).

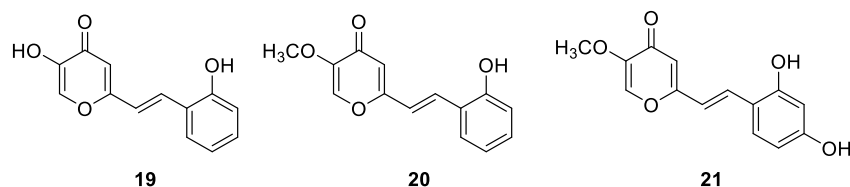
3.4. Synthesis of piranone phosphonium salt

The synthesis of 2-((chlorotriphenyl- λ^5 -phosphanyl)methyl)-5-methoxy-4*H*-pyran-4-one was carried out in three steps. In the first step, pyranone chloride was prepared as follows: 5-hydroxy-2-(hydroxymethyl)-4*H*-pyran-4-one (50.0 mmol) and DCM (82 mL) were added to a three-necked flask (250 mL) with a chlorine-calcium tube on one neck, and the mixture was cooled to 0 °C using an ice bath. Then, SOCl₂ (50.0 mmol, 1 eq) was added dropwise through the needle through the other neck, and the mixture was stirred for five hours, after which the solvent was evaporated, and the corresponding chloride remained in the flask. In the next step, 10% KOH (3 mL) was added to the prepared yellowish chloride (48.8 mmol) in a three-necked flask (250 mL) with a chlorine-calcium tube, and (CH₃)₂SO₄ (5 mL) was added dropwise via a needle. The mixture was stirred for one hour in an ice bath, after which another portion of 10% KOH (0.03 mL) was added, and then more (CH₃)₂SO₄ (5 mL) was added via needle. The resulting mixture was extracted with CHCl₃ (5 x 15 mL). A dark red solution was obtained as an organic layer, dried over MgSO₄, and filtered and evaporated on a rotary evaporator, after which a dark red oil remained. In the last step, the resulting chloride (24.81 mmol) was added to a three-necked flask (250 mL), and PPh₃ (24.81 mmol, 1 eq) dissolved in toluene (40 mL) was added. The mixture was heated to reflux temperature, and under these conditions, the reaction was carried out for four days, after which the reaction mixture was filtered under pressure and then dried in a desiccator for 12 h.

3.5. Synthesis of new piranone derivatives

Before carrying out the Wittig reaction, the apparatus was purged with nitrogen for 15 minutes. The reaction was carried out in a three-necked flask (250 mL), on the two side necks of which a chlorine-calcium tube and a balloon with N₂ were placed, connected via a syringe and a septum to the neck of the flask. A dropping funnel was attached to the middle neck of the flask, into which 50 mL of EtOH was added, and half the volume was drained into the flask, and the phosphonium salt (5.74 mmol, 1 eq, 5.07 mmol, 1 eq) was added, and in the remaining 25 mL of Na (1.1 eq) was added. The mixture was stirred until all the Na had reacted, and then aldehyde (5.74 mmol, 1 eq for compounds 19 and 20 and 5.07 mmol, 1 eq for compound 21) was added slowly dropwise with NaOEt. The reaction mixture was allowed to stir at room temperature for a certain time (72 h). The reaction mixture was then evaporated on a rotary evaporator to remove the ethanol, and after evaporation, the residual oil was dissolved and extracted with toluene (5 x 15 mL). The organic

layer was filtered through a pleated filter paper, dried over anhydrous MgSO₄, and then evaporated to a dry product. The *trans*-isomers of compounds **19-21** were isolated from the obtained raw products by successive column chromatography on silica gel, using PE/E and EtOAc/MeOH solvent systems of different polarities.



(*E*)-5-**H**ydroxy-2-(2-hydroxystyryl)-4*H*-pyran-4-on (**19**) [**27**]: 88 mg; orange powder, m. p. 185-186 °C; R_f (E) = 0.12; UV (ACN with small amount of MeOH) λ_{max}/nm ($\epsilon/dm^3mol^{-1}cm^{-1}$) 353 (29371); IR ν_{max}/cm^{-1} (NaCl): 3411, 3248, 1630, 1552, 1421, 1321, 1248, 1040, 963, 939; ¹H NMR (CD₃OD, 600 MHz) δ/ppm : 7.83 (s, 1H), 7.70 (d, J = 16.6 Hz, 1H), 7.51 (d, J = 7.4 Hz, 1H), 7.17 (t, J = 8.0 Hz, 1H), 7.00 (d, J = 16.3 Hz, 1H), 6.84 (t, J = 7.5 Hz, 3H); ¹³C NMR (DMSO, 75 MHz) δ/ppm : 144.2, 136.4, 131.9, 130.9, 128.5, 124.5, 124.2, 119.6, 116.3, 116.2, 105.1, 107.6, 99.4; MS (ESI) (m/z) (% , fragment): 231 (100); HRMS (m/z) for C₁₃H₁₀O₄: [M+H]⁺_{calculated} = 230.0579, [M+H]⁺_{measured} = 230.0583.

(*E*)-2-(2-**H**ydroxystyryl)-5-methoxy-4*H*-pyran-4-on (**20**): 60 mg, 8% isolated, yellow powder; m. p. 174-176 °C; R_f (EtOAc)= 0.18; UV (ACN) λ_{max}/nm ($\epsilon/dm^3mol^{-1}cm^{-1}$) 353 (17133), 276 (16184); ¹H NMR (CD₃OD, 600 MHz) δ/ppm : 7.97 (s, 1H), 7.75 (d, J = 16.5 Hz, 1H), 7.54 (d, J = 8.7 Hz, 1H), 7.19 (t, J = 8.7 Hz, 1H), 7.03 (d, J = 16.5 Hz, 1H), 6.88 – 6.85 (m, 2H), 6.52 (s, 1H), 1.29 (s, 3H); MS (ESI) (m/z) (% , fragment): 245 (5), 233 (100).

(*E*)-2-(2,4-**D**ihydroxystyryl)-5-methoxy-4*H*-pyran-4-on (**21**): 40 mg, 5% isolated; yellow powder, m. p. 181-183 °C R_f (EtOAc)= 0.08; UV (ACN) λ_{max}/nm ($\epsilon/dm^3mol^{-1}cm^{-1}$) 357 (10980); ¹H NMR (CD₃OD, 600 MHz) δ/ppm : 6.49 (s, 1H), 6.19 (d, J = 16.1 Hz, 1H), 5.87 (d, J = 8.5 Hz, 1H), 5.32 (d, J = 16.1 Hz, 1H), 4.85 (s, 1H), 4.83 – 4.81(m, 2H), 2.28 (s, 3H); ¹³C NMR (CD₃OD, 150 MHz) δ/ppm : 148.0, 138.4, 133.3, 131.7, 130.5, 129.4, 128.5, 114.5, 114.1, 112.2, 108.8, 107.6, 101.9, 29.4; MS (ESI) (m/z) (% , fragment): 261 (100), 166 (60); HRMS (m/z) for C₁₄H₁₂O₅: [M+H]⁺_{calculated} = 260.0685, [M+H]⁺_{measured} = 260.0684.

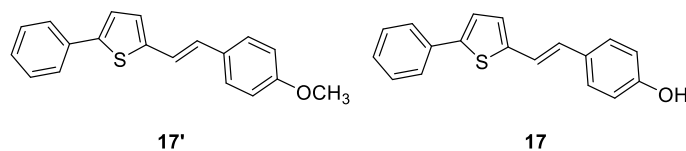
3.6. Synthesis of **17'** and **17**

4-Methoxytoluene (12.2 g), NBS (19.6 g), and AIBN (0.21 g) were added to a round flask (500 mL), and the mixture was heated under reflux to 100 °C. After the establishment of reflux, a color change to white was observed. After two hours of reflux, a change in the color of the solution to orange was observed, and the resulting succinimide floated on the solution's surface. The resulting succinimide was filtered off into a flask (250 mL), and the filtrate was evaporated to dryness. A red oil was obtained, which was dissolved in toluene (80 mL), and PPh₃ (26.23 g) was added. The reaction mixture was stirred at room temperature for 40 h. The next day, the reaction mixture was filtered through a Büchner funnel, and the obtained phosphonium salt was dried in a desiccator for 24 h.

Before carrying out the Wittig reaction, the apparatus was purged with nitrogen for 15 minutes. The reaction was carried out in a three-necked flask (250 mL), on the two side necks of which a chlor-calcium tube and a balloon with N₂ were placed, connected via a syringe and a septum to the neck of the flask. A dropping funnel was attached to the middle neck of the flask, into which 40 mL of EtOH was added, and half the volume was dropped into the flask. The prepared *p*-methoxy-phosphonium salt (0.97 mmol) was then added to the flask, and the mixture was stirred using a magnetic stirrer. Weighed Na (1.1 eq) was added to the remaining 20 mL of EtOH. The mixture was allowed to stir until all the Na had reacted. Then, aldehyde (1 eq) was added to the reaction mixture with NaOEt added dropwise, and the reaction mixture was left to stir for 72 h at room temperature. The mixture was then extracted with toluene, and the organic layer was dried over anhydrous MgSO₄, which serves as a drying agent. After 30 minutes of drying, the solvent was evaporated, and the organic product as a mixture of *cis*- and *trans*-isomers was purified on a column filled with silica gel. The solvent system PE/E with variable polarity was used as eluent. The pure *trans*-isomer of compound **17'** was isolated in the last fractions by subsequent column chromatography with the same solvent system.

Isolated **17'** (0.05 g) was added to a flask (250 mL) with DCM (0.045 mL). The flask was immersed in a bath with acetone and dry ice when the dry ice temperature of -78 °C was reached. A 1 M solution of BBr₃ in DCM (4 mL) was added with a glass syringe over one hour. After all the reagent was added, the flask was slowly lifted from the bath and stirred for 24 hours at room temperature. After 24 h of stirring, the flask was transferred to an ice bath and neutralized with 1 mol/L NaOH. The reaction mixture was extracted with EtOAc, and the organic layer was dried over MgSO₄.

After 30 minutes of drying, the solvent was evaporated, and the organic product was purified on a column filled with silica gel, where pure **17** was obtained. The solvent system PE/E with variable polarity was used as eluent.



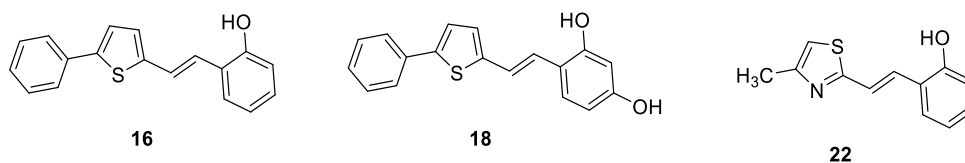
(*E*)-2-(4-Methoxy-styryl)-5-phenylthiophen (**17'**): 80 mg, 28% isolated; yellow powder; m. p. 125-127 °C; R_f (PE/E (50 %)) = 0.78; UV (ACN) λ_{\max}/nm ($\epsilon/\text{dm}^3\text{mol}^{-1}\text{cm}^{-1}$) 368 (37536), 266 (8433), 226 (13302); ^1H NMR (CDCl_3 , 600 MHz) δ/ppm : 7.61 (d, $J = 7.4$ Hz, 2H), 7.41 (d, $J = 8.9$ Hz, 2H), 7.38 (t, $J = 7.7$ Hz, 2H), 7.27 (t, $J = 7.7$ Hz, 1H), 7.21 (d, $J = 3.8$ Hz, 1H), 7.07 (d, $J = 16.6$ Hz, 1H), 6.98 (d, $J = 3.9$ Hz, 1H), 6.90 – 6.88 (m, 3H), 3.83 (s, 3H); ^{13}C NMR (CDCl_3 , 150 MHz) δ/ppm : 159.3, 142.7, 142.4, 134.3, 129.8, 128.9, 127.9, 127.6, 127.4, 126.6, 125.6, 123.5, 119.9, 114.2, 55.3; MS (ESI) (m/z) (% , fragment): 293 (100).

(*E*)-4-(2-(5-Phenylthiophen-2-yl)vinyl)phenol (**17**): 3 mg, 12% isolated; yellow powder; m. p. 85-90 °C; R_f (PE/E (70 %)) = 0.22; UV (ACN) λ_{\max}/nm ($\epsilon/\text{dm}^3\text{mol}^{-1}\text{cm}^{-1}$) 298 (83083); ^1H NMR (CDCl_3 , 600 MHz) δ/ppm : 7.54 (d, $J = 7.7$ Hz, 2H), 7.50 (d, $J = 8.7$ Hz, 2H), 7.34 – 7.29 (m, 3H), 7.11 (d, $J = 3.1$ Hz, 1H), 6.80 (d, $J = 8.3$ Hz, 2H), 6.78 (d, $J = 8.7$ Hz, 2H), 6.68 (d, $J = 3.1$ Hz, 1H), 4.81 (s, 1H); ^{13}C NMR (CDCl_3 , 150 MHz) δ/ppm : 147.8, 146.9, 146.4, 143.8, 142.5, 130.4, 129.4, 128.7, 127.1, 125.5, 125.2, 122.6, 115.4, 115.3; MS (ESI) (m/z) (% , fragment): 279 (100).

3.7. Synthesis of **16** and **18**

Compounds **16** and **18** were synthesized by the McMurry reaction. Before carrying out the reaction, the apparatus was purged with argon for 15 minutes. The reaction was carried out in a three-necked flask (250 mL) on a magnetic stirrer. Zinc powder (6.65 mmol) and THF (40 mL) were added to the flask. The reaction mixture was cooled to -5 °C, and TiCl_4 (3 mL) was added dropwise via syringe while maintaining the temperature below 0 °C. After that, the reaction mixture was heated to room temperature and stirred for 30 minutes. After 30 minutes, the reaction mixture was heated to the reflux temperature and left for 3 hours. When the reflux was stopped, a mixture of aldehydes (1.33 mmol, 1.2 eq, in a ratio of 1:1.2) in THF was added dropwise via needle to the reaction mixture after cooling (-5 °C). When the aldehydes were added, the reaction mixture was reheated

to reflux temperature and left for two hours. Afterward, it was cooled to room temperature and left overnight with stirring on a magnetic stirrer. The reaction mixture was then neutralized with aqueous NaHCO₃ solution. The neutralized reaction mixture was extracted with EtOAc (3 x 25 mL), and then the organic layer was dried over MgSO₄. After 30 minutes of drying, the solvent was evaporated, and the organic product was purified on a column filled with silica gel. PE/E and PE/DCM solvent systems of different polarities were used as eluents.



(*E*)-2-(2-(5-Phenylthiophen-2-yl)vinyl)phenol (**16**): 11 mg, 5% isolated; yellow powder; m. p. 113-115 °C; R_f (PE/DCM (30 %)) = 0.78; UV (ACN) λ_{\max}/nm ($\epsilon/\text{dm}^3\text{mol}^{-1}\text{cm}^{-1}$) 353 (6553), 234 (2149); ¹H NMR (CDCl₃, 600 MHz) δ/ppm : 7.64 (d, J = 8.3 Hz, 2H), 7.55 (d, J = 7.7 Hz, 1H), 7.49 (d, J = 8.4 Hz, 1H), 7.46 (d, J = 3.9 Hz, 1H), 7.41 (t, J = 7.9 Hz, 2H), 7.32 – 7.30 (m, 2H), 7.28 (t, J = 7.4 Hz, 1H), 7.23 (t, J = 7.6 Hz, 1H), 6.98 (s, 1H), 6.88 (d, J = 1.1 Hz, 1H); ¹³C NMR (CDCl₃, 150 MHz) δ/ppm : 154.6, 151.1, 144.7, 135.8, 133.9, 129.1, 129.0, 127.9, 125.8, 125.5, 124.4, 123.9, 123.2, 120.8, 111.0, 101.2; MS (ESI) (m/z) (% , fragment): 279 (100).

(*E*)-4-(2-(5-Phenylthiophen-2-yl)vinyl)benzene-1,3-diol (**18**): 6 mg, 10% isolated; yellow powder; m. p. 128-130 °C; R_f (PE/DCM (30 %)) = 0.69; ¹H NMR (CDCl₃, 300 MHz) δ/ppm : 7.54 (d, J = 7.1 Hz, 2H), 7.35 (t, J = 7.1 Hz, 3H), 7.26 – 7.21 (m, 3H), 7.10 (d, J = 3.9 Hz, 1H), 6.98 (s, 2H), 6.73 – 6.71 (m, 1H), 5.00 (s, 1H); ¹³C NMR (CDCl₃, 150 MHz) δ/ppm : 151.5, 141.9, 139.5, 135.8, 134.7, 130.0, 128.8, 128.3, 126.9, 126.2, 125.6, 125.5, 125.5, 125.4, 125.3, 122.9; MS (ESI) (m/z) (% , fragment): 295 (100).

(*E*)-2-(2-(2-Methylthiazol-5-yl)vinyl)phenol (**22**) [29]: 13 mg (isolated yield from the mixture 65%), yellow oil, R_f (PE/E = 80%) = 0.50; UV (ACN) λ_{\max}/nm ($\epsilon/\text{dm}^3\text{mol}^{-1}\text{cm}^{-1}$) 345 (sh, 6109), 332 (21,971), 315 (sh, 20036), 300 (sh, 19398), 285 (23,628); ¹H NMR (CDCl₃, 600 MHz) δ/ppm : 7.69 (d, J = 15.9 Hz, 1H), 7.47 (d, J = 7.4 Hz, 1H), 7.16–7.09 (m, 2H), 7.01 (s, 1H), 6.90 (t, J = 7.1 Hz, 1H), 6.79 (d, J = 8.6 Hz, 1H), 6.25 (s, 1H), 2.76 (s, 3H); ¹³C NMR (CDCl₃, 75 MHz) δ/ppm : 116.3, 154.2, 153.8, 128.8, 127.5, 126.0, 124.3, 122.5, 120.8, 116.1, 114.6, and 19.3; MS (ESI) m/z

(%, fragment): 218 (20); 158 (100); HRMS (m/z) for $C_{12}H_{11}NOS$: $[M + H]^+$ calcd = 217.0561, and $[M + H]^+$ measured = 217.0557.

3.8. Antioxidative activity of the new resveratrol derivatives

In this study, two methods were used for measuring the antioxidant activity of synthesized compounds: the most common DPPH radical scavenging activity assay and the additional Cuprac reducing antioxidant capacity test.

DPPH radical scavenging activity

The DPPH test of the synthesized compounds was measured using the method of Brand- Williams [37] using the stable radical, 2,2'-diphenyl-1-picrylhydrazyl (DPPH, Sigma-Aldrich, St. Louis, MO). The 50 μ L of various concentrations of tested solutions were added to 1 mL of etanolic solution of DPPH, and the final DPPH concentration was kept constant ($c = 8 \cdot 10^{-4}$ mol/L). After incubation of the reaction mixture for 30 minutes at 25 °C, a decrease in absorbance was measured at 517 nm (UV-1800 UV/Vis Spectrophotometer, Shimadzu, Japan). Inhibition of DPPH expressed in percentage was calculated according to the equation: Inhibition (%) = $[(A_{C(0)} - A_{A(t)}) / A_{C(0)}] \times 100$, where $A_{C(0)}$ is the absorbance of the control at $t = 0$ min, and $A_{A(t)}$ is the absorbance of the antioxidant at $t = 30$ min. All determinations were performed in triplicate. Inhibitions were represented as mean values \pm standard deviation. Data were used to calculate the IC_{50} value by a nonlinear fit of compound concentration values vs. inhibition percentage.

Cuprac reducing antioxidant capacity assay (CUPRAC)

The CUPRAC assay of the synthesized compounds was determined according to the method of Apak et al. [38]. Copper(II) chloride, neocuproine, ammonium acetate, and Trolox were purchased from Sigma-Aldrich (St. Louis, MO). To a test tube, 1 mL of each 10 mM Cu(II) chloride, 7.5 mM neocuproine (dissolved in ethanol), and NH_4Ac buffer (1 M, pH 7.0) were added. To an initial mixture x mL of testing sample (or standard Trolox) and $(1,1-x)$ mL of H_2O were added to make the final volume 4.1 mL. The tubes were stoppered, and after 30 min, the absorbance at 450 nm was recorded against a reagent blank containing no compound. The standard calibration curve of Trolox was constructed as the absorbance versus concentration graph. Molar absorptivity for each

antioxidant tested was found from the slope of the calibration line. CUPRAC values were expressed as a mole of Trolox equivalent (TE) per mole of the compound tested.

In vitro ChE activity assay

The acetylcholinesterase (AChE) and butyrylcholinesterase (BChE) inhibitions were determined using modified Ellman's method [34]. AChE (E.C. from electric eel), BChE (E.C. from equine serum), trisma base, acetylthiocholine iodide (ATChI), *S*-butyrylthiocholine iodide (BTChI) and galantamine were purchased from Sigma-Aldrich (St. Louis, MO), while 5,50-dithiobis-(2-nitrobenzoic acid) (DTNB, Ellman's reagent) was purchased from Zwijndrecht (Belgium). Galantamine was used as a reference standard. AChE/BChE activity was measured using a 96-well microplate reader (IRE 96, SFRI Medical Diagnostics) at room temperature at 405 nm over 6 min. Each well was filled with 180 μ L tris buffer (50 mM, pH 8.0), 10 μ L of an enzyme (AChE/BChE final concentration 0.03 U/mL, prepared in 20 mM Tris buffer, pH 7.5), and 10 μ L of tested solutions of different concentrations (final concentrations in a range 0.1–1000 μ M, depending on solubility) and 10 μ L of DTNB (final concentration 0.3 mM prepared in Tris buffer). The reaction was initiated by adding 10 μ L of ATChI/BTChI (final concentration of 0.5 mM prepared in Tris buffer). In the control measurement, the tested compound was replaced by a buffer solution. For each measurement, the non-enzymatic hydrolysis was measured as a blank where an equivalent buffer amount replaced the enzyme. The experiment was run in triplicate. Percentage enzyme inhibition was calculated according to the equation: $\text{Inhibition (\%)} = [(A_C - A_T) / A_C] \times 100$ where A_C is the enzyme activity without the test sample and A_T is the enzyme activity with the test sample and represented as mean values \pm standard deviation. Data of mean inhibition were used to calculate the IC_{50} value by a nonlinear fit of compound concentration values vs. response. Ethanol was used as a solvent. The inhibitory activity of ethanol was also measured, and its contribution to inhibition was subtracted.

3.9. Computational details

The ligands were prepared for the docking by geometry optimizations employing the Gaussian16 program package [39] at the M06-2X/6-31G(d) level of theory. The molecular docking study was performed using the Autodock program package [40]. The crystal structure of BChE (PDB code 1P0i) was taken from the Protein Data Bank [41]. Docking simulations were done utilizing the

Lamarckian Genetic Algorithm, generating 25 genetic algorithm dockings with 25 binding poses for each ligand with rigid residues of the enzymes during the docking. The most stable complexes between protein and ligand obtained by docking were used as starting structures for molecular dynamics study. A truncated octahedron of the OPC water box was used to solvate the protein-ligand complexes, and neutralization with Na⁺ ions using the Amber16 program package was done [42], with the ff14SB force field [43] for the protein part of the enzyme, and the GAFF force field [44] for ligands. Partial charges for ligands were derived using the RESP procedure. Equilibrations of all four systems involved energy minimizations and short (20 ps) MD simulations with systematic decreases to zero of the harmonic restraints and relaxation of the volume and temperature with target values of the temperature and pressure set to 300 K and 1 atm, respectively. Production MD simulation with no constraints was performed in the duration of 100 nanoseconds under NPT conditions (300 K and 1 atm).

3.10. X-ray crystallographic study

Single crystal measurements on a dual source (Mo/Cu) Rigaku Oxford Diffraction Synergy S diffractometer equipped with an Oxford Cryosystems Series 800 cryostat. The program package CrysAlis PRO [45] was used for data reduction and numerical absorption correction. The structures were solved using SHELXS97 [46] and refined with SHELXL-2017 [47]. Models were refined using the full-matrix least-squares refinement; all non-hydrogen atoms were refined anisotropically. Hydrogen atoms were located in a different Fourier map and refined as riding entities.

Molecular geometry calculations were performed by PLATON [48], and molecular graphics were prepared using ORTEP-3 [49] and Mercury [50]. Crystallographic and refinement data for the structures reported in this paper are shown in Table 5.

Table 5. Crystallographic, data collection, and refinement data.

Compound	5	14
Empirical formula	C ₃₆ H ₃₀ O ₃ S ₃	C ₁₄ H ₁₄ O ₂ S
Formula wt. / g mol ⁻¹	606.83	246.31
Colour	colourless	colourless

Crystal dimensions / mm	0.20 x 0.15 x 0.10	0.11 x 0.06 x 0.04
Space group	$P 2_1 2_1 2$	$P bca$
$a / \text{\AA}$	15.8330(4)	8.6581(6)
$b / \text{\AA}$	33.3810(8)	18.9936(17)
$c / \text{\AA}$	5.9700(2)	14.9550(16)
$\alpha / ^\circ$	90	90
$\beta / ^\circ$	90	90
$\gamma / ^\circ$	90	90
Z	4	8
$V / \text{\AA}^3$	3155.27(15)	2459.3(4)
$D_{\text{calc}} / \text{g cm}^{-3}$	1.277	1.291
$\lambda / \text{\AA}$	1.54179 (CuK α)	1.54179 (CuK α)
μ / mm^{-1}	2.384	2.227
Θ range / $^\circ$	3.09 – 77.03	5.52 – 77.15
T / K	293(2)	293(2)
Diffractometer type	Synergy S	Synergy S
Range of h, k, l	$-20 < h < 17;$ $-41 < k < 40;$ $-7 < l < 3$	$-10 < h < 10;$ $-22 < k < 22;$ $-15 < l < 18$
Reflections collected	12372	7727
Independent reflections	5547	2359
Observed reflections ($I \geq 2\sigma$)	4622	1409
Absorption correction	Multi-scan	Multi-scan
$T_{\text{min}}, T_{\text{max}}$	0.8148; 1.0000	0.0422; 1.0000
R_{int}	0.0261	0.1672
$R (F)$	0.1097	0.1261
$R_w (F^2)$	0.3455	0.3219

Goodness of fit	1.491	1.065
H atom treatment	Constrained	Constrained
No. of parameters	383	158
No. of restraints	55	0
$\Delta\rho_{\max}$, $\Delta\rho_{\min}$ ($\text{e}\text{\AA}^{-3}$)	0.922; -0.547	0.876; -0.644

4. Conclusions

In this study, we synthesized novel heterocyclic derivatives based on the well-known biologically active compound *trans*-resveratrol. These derivatives were prepared using either the Wittig or the McMurry reaction, resulting in mixtures of *cis*- and *trans*-isomers. The pure *trans*-isomers of interest were then isolated and characterized using NMR, UV-Vis spectrophotometry, and mass spectrometry. Furthermore, biological testing on these newly synthesized resveratrol analogs was conducted. Several of these derivatives exhibited significantly enhanced inhibitory and antioxidant activity compared to established standards such as galantamine or resveratrol. To gain insights into the molecular interactions, we performed molecular docking studies of selected ligands into BChE, which revealed that the tested resveratrol derivatives displayed an affinity for forming hydrogen bonds with residues in the active site, as well as engaging in π - π stacking and hydrophobic interactions. Molecular dynamics (MD) simulations further validated the resulting complexes' stability. Additionally, Lhasa software was employed to identify potential mutagenicity among the heterocyclic resveratrol analogs. While five structures showed some potential for mutagenicity, it is worth noting that none of them ranked among the most active molecules identified in our study.

Supplementary Materials: Supplementary Material contains NMR spectra, mass spectra, and HRMS analyses of compounds **1-22**, X-Ray analyses data, Cartesian coordinates of docked ligands, free energies of binding obtained by docking (Table S1), RMSD, RMSF, and Rg for protein-ligand complexes derived by MD simulation (Table S2).

Acknowledgments: This work was supported by grants from the University of Zagreb short-term scientific support for 2022 under the title *Experimental and computational studies of new heterocyclic o-divinylbenzenes* and by Federal Ministry of Education and Science, Bosnia and Herzegovina, Grant No. 05-35-2046-1/22. We thank the University of Zagreb Computing Centre

(SRCE) for granting computational time on the ISABELLA cluster. We also acknowledge the NMR Centre at RBI for recording all the NMR spectra.

References

1. Abbasa, M.; Saeeda, F.; Anjuma, F.M.; Afzaala, M.; Tufaila, T.; Bashirb, M.S.; Ishtiaqb, A.; Hussainc, S.; Suleria, H.A.R. Natural polyphenols: An overview, *Int. J. Food Prop.* **2017**, *20*, 1689–1699. <https://doi.org/10.1080/10942912.2016.1220393>
2. Manach, C.; Scalbert, A.; Morand, C.; Re'me'sy, C.; Jimenez, L. Polyphenols: food sources and bioavailability, *Am. J. Clin. Nutr.* **2004**, *79*, 72747. <https://doi.org/10.1093/ajcn/79.5.727>
3. Aluko, R.E. Functional foods and nutraceuticals, *Food science text series*, **2012**. New York, NY: Springer Publishers
4. Han, X.; Shen, T.; Lou, H. Dietary polyphenols and their biological significance, *Int. J. Mol. Sci.* **2007**, *8*, 950–988. <https://doi.org/10.3390/i8090950>
5. Giacomini, E.; Rupiani, S.; Guidotti, L.; Recanatini, M.; Roberti, M. The use of stilbene scaffold in medicinal chemistry and multi-target drug design, *Curr. Med. Chem.* **2016**, *23*, 2439–2489.
6. Belwal, T.; Nabavi, S.M.; Nabavi, S.F.; Dehpour, A.R.; Shirooie, S. Naturally occurring chemicals against Alzheimer's Disease, Academic, **2020**. London. <https://doi.org/10.1016/C2018-0-03965-1>
7. Thimmappa, S.A. Resveratrol-a boon for treating Alzheimer's disease? *Brain Res. Rev.* **2006**, *52*, 316–326. <https://doi.org/10.1016/j.brainresrev.2006.04.004>
8. Martelli, D.; McKinley, M.J.; McAllen, R.M. The cholinergic anti-inflammatory pathway: a critical review, *Auton. Neurosci.* **2014**, *182*, 65–69. <https://doi.org/10.1016/j.autneu.2013.12.0078>
9. Stervbo, U.; Vang, O.; Bonnesen, C. A review of the content of the putative chemopreventive phytoalexin resveratrol in red wine, *Food Chem.* **2007**, *101*, 449–457. <https://doi.org/10.1016/j.foodchem.2006.01.047>
10. Fornara, V.; Onelli, E.; Sparvoli, F.; Rossoni, M.; Aina, R.; Marino, G.; Citterio, S. Localization of stilbene synthase in *Vitis vinifera* L. during berry development, *Protoplasma* **2008**, *233*, 83–93. <https://doi.org/10.1007/s00709-008-0309-8>
11. Sousa, J.C.E.; Santana, A.C.F.; Magalhães, G.J.P. Resveratrol in Alzheimer's disease: a review of pathophysiology and therapeutic potential, *Arq. Neuro-Psiquiatr.* **2020**, *78*, 501–511. <https://doi.org/10.1590/0004-282X20200010>

12. Di Lorenzo, C.; Colombo, F.; Biella, S.; Stockley, C.; Restani, P. Polyphenols and human health: the role of bioavailability, *Nutrients* **2021**, *13*, 273. <https://doi.org/10.3390/nu13010273>
13. Gomez Silva, C.; Monteiro, J.; Marques, R.R.N.; Silva, A.M.T.; Martínez, C.; Canle, L.; Faria, J.L. Photochemical and photocatalytic degradation of trans-resveratrol, *Photochem. Photobiol. Sci.* **2013**, *12*, 638–644. <https://doi.org/10.1039/C2PP25239B>
14. Richardson, F.S.; Riehl, J.P. Circularly polarized luminescence spectroscopy, *Chem. Rev.* **1977**, *77*, 773–792. <https://doi.org/10.1021/cr60310a001>
15. Galano, A.; Álvarez-Diduk, R.; Ramírez-Silva, M.T.; Alarcón-Ángeles, G.; Rojas-Hernández, A. Role of the reacting free radicals on the antioxidant mechanism of curcumin, *Chem. Phys.* **2009**, *363*, 13–23. <https://doi.org/10.1016/j.chemphys.2009.07.003>
16. Soobrattee, M.A.; Neergheen, V.S.; Luximon-Ramma, A.; Aruoma, O.I.; Bahorun, T. Phenolics as potential antioxidant therapeutic agents: mechanism and actions, *Mutat. Res.* **2005**, *579*, 200–213. <https://doi.org/10.1016/j.mrfmmm.2005.03.023>
17. Jang, J.H.; Surh, Y.J. Protective effect of resveratrol on beta-amyloid-induced oxidative PC12 cell death, *Free Radic. Biol. Med.* **2003**, *34*, 1100–1110. [https://doi.org/10.1016/S0891-5849\(03\)00062-5](https://doi.org/10.1016/S0891-5849(03)00062-5)
18. He, S.; Yan, X. From resveratrol to its derivatives: new sources of natural antioxidant, *Curr. Med. Chem.* **2013**, *20*, 1005. <https://doi.org/10.2174/092986713805288941>
19. Freskgård, P.O.; Urich E. Antibody therapies in CNS diseases, *Neuropharm.* **2017**, *120*, 38–55. <https://doi.org/10.1016/j.neuropharm.2016.03.014>
20. Marambaud, P.; Zhao, H.; Davies, P. Resveratrol promotes clearance of Alzheimer's disease amyloid-beta peptides, *J. Biol. Chem.* **2005**, *280*, 37377–37382. <https://doi.org/10.1074/jbc.M508246200>
21. Vingtdeux, V.; Dreses-Werringloer, U.; Zhao, H.; Davies, P.; Marambaud, P. Therapeutic potential of resveratrol in Alzheimer's disease, *BMC Neurosci.* **2008**, *9*, 6. <https://doi.org/10.1186/1471-2202-9-S2-S6>
22. Lange, K.W.; Li, S. Resveratrol, pterostilbene, and dementia, *BioFactors* **2018**, *44*, 83–90. <https://doi.org/10.1002/biof.1396>
23. Braidy, N.; Jugder, B.E.; Poljak, A.; Jayasena, T.; Mansour, H.; Nabavi, S.M.; Sachdev, P.; Grant, R. Resveratrol as a potential therapeutic candidate for the treatment and management of Alzheimer's disease, *Curr. Top. Med. Chem.* **2016**, *16*, 1951–1960.

24. Bastianetto, S.; Ménard, C.; Quirion R. Neuroprotective action of resveratrol, *Biochim. Biophys. Acta* **2015**, *1852*, 1195–1201. <https://doi.org/10.1016/j.bbadis.2014.09.011>
25. Pasinetti, G.M.; Wang, J.; Ho, L.; Zhao, W.; Dubner, L. Roles of resveratrol and other grape-derived polyphenols in Alzheimer's disease prevention and treatment, *Biochim. Biophys. Acta* **2015**, *1852*, 1202–1208. <https://doi.org/10.1016/j.bbadis.2014.10.006>
26. Kulkarni, S.S.; Cantó, C.; The molecular targets of resveratrol, *Biochim. Biophys. Acta* **2015**, *1852*, 1114–1123. <https://doi.org/10.1016/j.bbadis.2014.10.005>
27. Mlakić, M.; Fodor, L.; Odak, I.; Horváth, O.; Lovrić, M.J.; Barić, D.; Milašinović, V.; Molčanov, K.; Marinić, Ž.; Lasić, Z.; Škorić, I. Resveratrol-maltol and resveratrol-thiophene hybrids as cholinesterase inhibitors and antioxidants: synthesis, biometal chelating capability and crystal structure, *Molecules* **2022**, *27*, 6379. <https://doi.org/10.3390/molecules27196379>
28. Mlakić, M.; Rajić, L.; Ljubić, A.; Vušak, V.; Zelić, B.; Gojun, M.; Odak, I.; Čule, I.; Šagud, I.; Šalić, A.; Škorić, I. Synthesis of new heterocyclic resveratrol analogues in milli- and microreactors: Intensification of the Wittig reaction, *J. Flow Chem.* **2022**, *12*, 429–440. <https://doi.org/10.1007/s41981-022-00239-9>
29. Mlakić, M.; Đurčević, E.; Odak, I.; Barić, D.; Juričević, I.; Šagud, I.; Burčul, F.; Lasić, Z.; Marinić, Ž.; Škorić, I. Thieno-thiazolostilbenes, thienobenzo-thiazoles, and naphtho-oxazoles: Computational study and cholinesterase inhibitory activity, *Molecules* **2023**, *28*, 3781. <https://doi.org/10.3390/molecules28093781>
30. Horspool, W.M.; Song, P.S. CRC Handbook of Organic Photochemistry and Photobiology, Boca Raton, **1995**.
31. Griesbeck, A.; Oelgemöller, M.; Ghetti, F. CRC Handbook of Organic Photochemistry and Photobiology, third ed., Boca Raton, **2012**.
32. Gülçin, I. Antioxidant properties of resveratrol: A structure-activity insight, *Innov. Food Sci. Emerg.* **2010**, *11*, 210–218. <https://doi.org/10.1016/j.ifset.2009.07.002>
33. Fauconneau, B.; Waffo-Tegu, P.; Huguet, F.; Barrier, L.; Decendit, A.; Merillon, J.M. Comparative study of radical scavenger and antioxidant properties of phenolic compounds from *Vitis vinifera* cell cultures using in vitro tests, *Life Sci.* **1997**, *61*, 2103–2110. [https://doi.org/10.1016/s0024-3205\(97\)00883-7](https://doi.org/10.1016/s0024-3205(97)00883-7)

34. Ellman, G.L.; Courtney, K.C.; Andreas, V.; Feather-Stone, R.M. A new and rapid colorimetric determination of acetylcholinesterase activity, *Biochem. Pharmacol.* **1961**, *7*, 88–95. [https://doi.org/10.1016/0006-2952\(61\)90145-9](https://doi.org/10.1016/0006-2952(61)90145-9)
35. Hasselgren, C.; Bercu, J.; Cayley, A.; Cross, K.; Glowienke, S.; Kruhlak, N.; Muster, W.; Nicolette, J.; Vijayaraj Reddy, M.; Saiakhov, R.; Dobo, K. Management of pharmaceutical ICH M7 (Q)SAR predictions – The impact of model updates, *Regul. Toxicol. Pharmacol.* **2020**, *118*, 104807. <https://doi.org/10.1016/j.yrtph.2020.104807>
36. Scientific committee on consumer safety SCCS, Opinion on hair dye 1,2,4-trihydroxybenzene (1,2,4-THB) COLIPA n° A33, Submission VI. https://health.ec.europa.eu/system/files/2021-08/sccs_o_222_0.pdf, 2019 (adopted 20-21 June 2019).
37. Brand-Williams, W.; Cuvelier, M.E.; Berset, C. Use of a free radical method to evaluate antioxidant activity, *Food Sci. Technol.* **1995**, *28*, 25–30. [https://doi.org/10.1016/S0023-6438\(95\)80008-5](https://doi.org/10.1016/S0023-6438(95)80008-5)
38. Apak, R.; Güçlü, K.; Özyürek, M.; Karademir, S.E. Novel Total Antioxidant Capacity Index for Dietary Polyphenols and Vitamins C and E, Using Their Cupric Ion Reducing Capability in the Presence of Neocuproine: CUPRAC Method, *J. Agric. Food Chem.* **2004**, *52*, 7970–7981. <https://doi.org/10.1021/jf048741x>
39. Frisch, M.J.; Trucks, G.W.; Schlegel, H.B.; Scuseria, G.E.; Robb, M.A.; Cheeseman, J.R.; Scalmani, G.; Barone, V.; Petersson, G.A.; Nakatsuji, H.; et al. Gaussian 16; Revision C.01; Gaussian, Inc.: Wallingford, CT, USA, 2016.
40. Morris, G.M.; Huey, R.; Lindstrom, W.; Sanner, M.F.; Belew, R.K.;Goodsell, D.S.; Olson, A.J. AutoDock4 and AutoDock-823 Tools4: Automated docking with selective receptor flexibility. *J. Comput. Chem.* 2009, *16*, 2785–2791. <https://doi.org/10.1002/jcc.21256>
41. Nicolet, Y., Lockridge, O., Masson, P., Fontecilla-Camps, J.C., Nachon, F. Crystal structure of human butyrylcholinesterase. PDB DOI: <https://doi.org/10.2210/pdb1p0i/pdb>
42. Case, D. A.; Ben-Shalom, I. Y.; Brozell, S. R.; Cerutti, D. S.; Cheatham, III; T. E.; Cruzeiro, V. W. D.; Darden, T. A.; Duke, R. E.; Ghoreishi, D.; Gilson, M. et al. (2016), AMBER 2016, University of California, San Francisco.

43. Maier, J. A.; Martinez, C.; Kasavajhala, K.; Wickstrom, L.; Hauser, K. E.; Simmerling, C. ff14SB: Improving the Accuracy of Protein Side Chain and Backbone Parameters from ff99SB. *J. Chem. Theory Comput.* **2015**, *11*, 3696–3713. <https://doi.org/10.1021/acs.jctc.5b00255>
44. Wang, J.; Wolf, R. M.; Caldwell, J. W.; Kollman, P. A.; Case, D. A. Development and Testing of a General Amber Force Field. *J. Comput. Chem.*, **2004**, *25*, 1157–1174. <https://doi.org/10.1002/jcc.20035>
45. Rigaku, O.D. CrysAlis Pro V.40, Rigaku Oxford Diffraction Ltd, Yarnton, England, **2021**.
46. Sheldrick, G.M. SHELXTL – integrated space-group and crystal-structure determination, *Acta Crystallogr.* **2015**, *A71*, 3–8. <https://doi.org/10.1107/s2053273314026370>
47. Sheldrick, G.M. Crystal structure refinement with SHELXL, *Acta Crystallogr.* **2015**, *C71*, 3–8. <https://doi.org/10.1107/s2053229614024218>
48. Spek, A.L. CheckCIF validation ALERTS: what they mean and how to respond, *Acta Crystallogr.* **2020**, *E76*, 1–11. <https://doi.org/10.1107/S2056989019016244>
49. Farrugia, L.J. ORTEP-3 for Windows – a version of ORTEP-III with a graphical user interface (GUI), *J. Appl. Cryst.* **1997**, *30*, 565. <https://doi.org/10.1107/S0021889897003117>
50. Macrae, C.F.; Sovago, I.; Cottrell, S.J.; Galek, P.T.A.; McCabe, P.; Pidcock, E.; Platings, M.; Shields, G.P.; Stevens, J.S.; Towler, M.; Wood, P.A. Mercury 4.0: from visualization to analysis, design and prediction, *J. Appl. Cryst.* **2020**, *53*, 226–235. <https://doi.org/10.1107/S1600576719014092>